

A dual-time-scale finite element model for simulating cyclic deformation of polycrystalline alloys

S Manchiraju, M Asai, and S Ghosh*

Department of Mechanical Engineering, Ohio State University, Columbus, Ohio

The manuscript was received on 26 April 2006 and was accepted after revision for publication on 22 January 2007.

DOI: 10.1243/03093247JSA233

Abstract: A dual-time-scale finite element model is developed in this paper for simulating cyclic deformation in polycrystalline alloys. The material is characterized by crystal plasticity constitutive relations. The finite element formulation of the initial boundary-value problems with cyclic loading involves decoupling the governing equations into two sets of problems corresponding to two different time-scales. One is a long-time-scale (low-frequency) problem characterizing a cycle-averaged solution, while the other is a short-time-scale (high-frequency) problem for a remaining oscillatory portion. Cyclic averaging together with asymptotic expansion of the variables in the time domain forms the basis of the multitime-scaling. The crystal plasticity equations at the two scales are used to study cyclic deformation of a titanium alloy Ti-6Al. This model is intended to study the fatigue response of a material by simulating a large number of cycles to initiation.

Keywords: cyclic deformation, crystal plasticity, multi-time-scale

1 INTRODUCTION

Many metals and alloys find widespread utilization in various high-performance applications such as automotive and aerospace components. Developments in advanced materials have contributed tremendously to the design and implementation of components with improved properties and reliability. During service, many of these components are exposed to cyclic loading conditions owing to start-up and shutdown processes or load reversals. In many cases, this results in their fatigue or time-delayed fracture. Fatigue failure in the microstructure evolves in three stages [1]:

- (a) crack nucleation due to inhomogeneous plastic flow or grain boundary failure;
- (b) subsequent crack growth by cyclic stresses;
- (c) coalescence of cracks to cause fast crack propagation.

The phenomena of high-cycle and low-cycle fatigue have been traditionally characterized using macroscopic parameters such as applied stresses, cyclic frequency, loading waveform, hold time, etc., as well as statistical distributions of fatigue life and fatigue strength [1–5]. Fatigue design by total life approaches includes the stress–life or S – N approach and the strain–life approach, e.g. the Coffin–Manson rule. Initiation of a fatigue crack and propagation to failure have been the prime objectives of these models. The total life approaches have been adjusted for notch effects using fatigue strength reduction and for variable amplitude fatigue, e.g. in the Palmgren–Miner rule of cumulative damage. In all cases, microstructural effects are represented by shifts in such data curves after extensive testing. Alternatively, the defect or damage tolerance approaches determine fatigue life as the number of cycles to propagate a crack from a certain initial size to a critical size. These are determined from threshold stress intensity, fracture toughness, limit load, allowable strain, or allowable compliance. The models assume the presence of a flaw in the structure and predict life using laws such as Paris law [6]. Fatigue crack

* Corresponding author: Department of Mechanical Engineering, Ohio State University, 650 Ackerman Road, Columbus, OH, 43202, USA. email: ghosh.5@osu.edu

advance has been conventionally based on linear elastic fracture mechanics analysis related to the concepts of similitude, in which stress intensity factors uniquely characterize fatigue crack growth. Although these models have worked well for alloys under specific test conditions, a lack of underlying physics- and microstructure-based considerations impede their portability to generic materials and load conditions.

Microstructural features, which include morphological and crystallographic characteristics, e.g. crystal orientations and misorientations, grain boundary geometry, etc., govern the mechanical behaviour and fatigue failure response. Recent years have seen a paradigm shift towards the use of detailed micromechanical models to understand damage mechanisms leading to fatigue failure. Crystal plasticity theories with explicit grain structures are effective in predicting localized cyclic plastic strains [7, 8]. Studies on deformation modelling [9] have established that preferred grain orientations due to crystal rotation facilitate slip transmittal across grain boundaries and are a dominant cause of material flow anisotropy leading to failure. In the crystallographic approach, the mechanical response of polycrystalline aggregates is deduced from the behaviour of constituent crystal grains, with specific assumptions about their interaction. Various computational studies have modelled anisotropy and its evolution in large deformation processes with the crystallographic approach [10–14]. Recent years have seen significant efforts in modelling cyclic plasticity and fatigue with consideration of microstructural stress–strain evolution. Finite element calculations have shown that, depending on the loading conditions, significant gradients of stress can arise within a single grain. Ghosh and co-workers have developed crystal plasticity models for deformation and creep in titanium alloys like Ti–6Al and Ti–6242 [15–17], and also models of deformation and ratcheting fatigue of HSLA steels [18–20]. Dawson and co-workers [21, 22] have investigated the mechanical behaviour of aluminium alloy in cyclic loading using crystal plasticity based FEM simulations of crystalline aggregates. McDowell and co-workers have incorporated a crystal plasticity model with kinematic hardening in ABAQUS to model cyclic plasticity in high-cycle fatigue in Ti–6Al–4V [8]. Modelling cyclic deformation using conventional time increments can be an exorbitant task for crystal plasticity computations. Most simulations performed with three-dimensional crystal plasticity are in the range of 100 cycles [8, 20–22], and the results are subsequently extrapolated for fatigue predictions. In

modelling fatigue, however, it is desirable to conduct simulations for a significantly high number of cycles to reach local states of damage initiation and growth. Conventional methods of time integration using semi-discretization present numerous challenges owing to the variation in time-scales ranging from the scale of the entire process to the time resolution required by the damage evolution and crack propagation. Yu and Fish [23] proposed a temporal homogenization method in which they assumed all the variables to be locally periodic in the temporal domain. However, for a deformation with evolving plastic variables, periodicity in the temporal domain cannot be assumed. This assumption was nominally relaxed in reference [24] to include variables that are almost periodic in time. The assumption of near-periodicity is not valid for most evolving microstructural variables in crystal plasticity simulations. In addition, this method invokes two-way coupling between the time-scales which requires having to solve initial value problems in each step at both time-scales. This can result in very high computational time and may not provide any advantage over single-time-scale calculations.

A method of solution of crystal plasticity equations is developed in this paper using two time-scales involving compression and rarefaction. From the set of crystal plasticity based governing equations, it develops a decoupled set of equations characterized by the two time-scales. One is a long-time-scale (low-frequency) problem characterizing a cycle-averaged solution, while the other is a short-time-scale (high-frequency) problem for a remaining oscillatory portion. Cyclic averaging together with asymptotic expansion of the variables in the time domain forms the basis of the multitime-scaling. The crystal plasticity equations at the two scales are used to study cyclic deformation of a titanium alloy Ti–6Al. The multitime-scaling results in an enormous gain (by a factor of about 50) in computational efficiency over single time integration with almost no loss of accuracy.

2 CRYSTAL PLASTICITY CONSTITUTIVE RELATIONS

The materials studied in this work are crystals with a hexagonal close-packed, or hcp, structure, e.g. titanium alloys consisting of five different families of slip systems as described in reference [15]. These include (a) three families of $\langle a \rangle$ systems, namely three equivalent basal $\{0001\}\langle 11\bar{2}0 \rangle$, three equivalent prismatic $\{10\bar{1}0\}\langle 11\bar{2}0 \rangle$, and six equivalent pyramidal

$\{10\bar{1}1\}\langle 11\bar{2}0\rangle$ systems, and (b) two families of pyramidal $\langle c+a\rangle$ systems, namely 12 first-order $\{10\bar{1}1\}\langle 11\bar{2}3\rangle$ and six second-order $\{11\bar{2}2\}\langle 11\bar{2}3\rangle$ systems. This constitutes a total of 30 possible slip systems for hcp crystals. In Ti alloys, the different slip systems exhibit strong anisotropic behaviour both in elasticity and in plasticity. For elasticity, a transversely isotropic response with five independent elastic constants is used [15–17, 25]. Plastic deformation occurs by crystallographic slip on the different slip systems. The deformation behaviour of the hcp material in this paper is modelled using a rate-dependent, isothermal, elastic–viscoplastic, finite strain, crystal plasticity formulation [15–17, 25]. In this model, crystal deformation results from a combination of elastic stretching and rotation of the crystal lattice and plastic slip on the different slip systems. The stress–strain relation is written in terms of the second Piola–Kirchhoff stress \mathbf{S} and the work conjugate Lagrange–Green strain tensor \mathbf{E} as

$$\mathbf{S} = \mathbf{C} : \mathbf{E}^e, \quad \text{where } \mathbf{E}^e = \frac{1}{2}(\mathbf{F}^{eT}\mathbf{F}^e - \mathbf{I}) \quad (1)$$

Here, \mathbf{C} is a fourth-order anisotropic elasticity tensor and \mathbf{F}^e is the elastic component of the deformation gradient which is obtained by multiplicative decomposition

$$\mathbf{F} = \mathbf{F}^e \mathbf{F}^p, \quad \det(\mathbf{F}^e) > 0 \quad (2)$$

where \mathbf{F} is the deformation gradient tensor and \mathbf{F}^p is its plastic component with the incompressibility constraint $\det(\mathbf{F}^p) = 1$. The flow rule governing evolution of plastic deformation is expressed in terms of the plastic velocity gradient as

$$\mathbf{L} = \dot{\mathbf{F}}^p \mathbf{F}^{p-1} = \sum_{\alpha}^{n_{\text{slip}}} \dot{\gamma}^{\alpha} \mathbf{s}^{\alpha} \quad (3)$$

where the Schmidt tensor associated with the α th slip system, \mathbf{s}^{α} , is expressed in terms of the slip direction, \mathbf{m}_0^{α} , and slip plane normal, \mathbf{n}_0^{α} , in the reference configuration as $\mathbf{s}^{\alpha} = \mathbf{m}_0^{\alpha} \otimes \mathbf{n}_0^{\alpha}$. For the plastic shearing rate $\dot{\gamma}^{\alpha}$ on slip system α , power-law descriptions have been described in a number of crystal plasticity models [10, 12, 26] as

$$\dot{\gamma}^{\alpha} = \dot{\gamma}_0 \left| \frac{\tau^{\alpha}}{g^{\alpha}} \right|^{1/m} \text{sign}(\tau^{\alpha}), \quad \tau^{\alpha} = (\mathbf{F}^{eT} \mathbf{F}^e \mathbf{S}) : \mathbf{s}^{\alpha} \quad (4)$$

where $\dot{\gamma}_0$ is a reference plastic shearing rate, τ^{α} is the resolved shear stress, g^{α} is the slip system resistance, and m is a material rate sensitivity parameter. The resistance parameters g^{α} are taken to evolve as

$$\dot{g}^{\alpha} = \sum_{\beta}^{n_{\text{slip}}} h^{\alpha\beta} |\dot{\gamma}^{\beta}| \quad (5)$$

The moduli $h^{\alpha\beta} = q^{\alpha\beta} h^{\beta}$ (no sum on β) correspond to the strain hardening rate due to self- and latent

hardening on the α th slip system owing to slip on the β th slip system. Here, h^{β} correspond to the self-hardening, and $q^{\alpha\beta}$ is a matrix describing the latent hardening. The evolution of self-hardening is expressed in terms of the equation

$$h^{\beta} = h_0 \left| 1 - \frac{g^{\beta}}{g_s^{\beta}} \right|^r \text{sign} \left(1 - \frac{g^{\beta}}{g_s^{\beta}} \right), \quad g_s^{\beta} = g_{s0} \left(\left| \frac{\dot{\gamma}^{\beta}}{\dot{\gamma}_0} \right| \right)^c \quad (6)$$

where h_0 is the initial hardening rate, g_s^{β} is the saturation slip deformation resistance, and r , g_{s0} , and c are the slip system hardening parameters.

For modelling of cyclic deformation it is important to include kinematic hardening. This has been done by including a back stress in power-law equation (4), as in references [15], [18], [19], [27], and [28]. The resolved effective stress $\tau_{\text{eff}}^{\alpha}$, which is the driving force for the dislocation motion on slip system α , is defined as

$$\tau_{\text{eff}}^{\alpha} = |\tau^{\alpha} - \tau_{\text{kin}}^{\alpha}| \quad (7)$$

where $\tau_{\text{kin}}^{\alpha}$ is the projection of the back stress tensor on slip system α

$$\tau_{\text{kin}}^{\alpha} = (\boldsymbol{\sigma}_{\text{kin}} \cdot \mathbf{n}^{\alpha}) \cdot \mathbf{m}^{\alpha} \quad (8)$$

The vectors $\mathbf{m}^{\alpha} (= \mathbf{F}^e \mathbf{m}_0^{\alpha})$ and $\mathbf{n}^{\alpha} (= \mathbf{F}^{e-T} \mathbf{n}_0^{\alpha})$ represent the slip direction and the normal to the slip plane, both of which evolve with deformation. As discussed in references [19] and [27], the back stress tensor is expressed in terms of scalar kinematic variables Ω^{α} as

$$\boldsymbol{\sigma}_{\text{kin}} = \sum_{\alpha} \Omega^{\alpha} (\mathbf{m}^{\alpha} \otimes \mathbf{n}^{\alpha} + \mathbf{n}^{\alpha} \otimes \mathbf{m}^{\alpha}) \quad (9)$$

where the components of Ω^{α} evolve owing to the short-range dislocation interactions as

$$\dot{\Omega}^{\alpha} = c\dot{\gamma}^{\alpha} - d\Omega^{\alpha} |\dot{\gamma}^{\alpha}| \quad (10)$$

In equation (10), c and d are the direct hardening and dynamic recovery coefficients respectively. Equation (9) takes into account the effect of back stress evolution of one system on all the other systems. The calibrated material constants are listed in Tables 1 and 2. Table 1 lists the elastic constants while Table 2 lists the crystal plasticity material constants.

3 DECOMPOSITION OF CONSTITUTIVE VARIABLES INTO AVERAGED AND OSCILLATOR PARTS

To illustrate the characteristics of plastic deformation of polycrystalline solids in response to cyclic loading, a crystal plasticity finite element (CPFE) simulation of

the Ti-6Al alloy is conducted. The problem is solved using a single-time-scale integration scheme in which each time increment is only a very small fraction of the load cycle period. A sinusoidally varying load is applied on a unit cube of the polycrystalline material in this CPFÉ simulation. The plastic strain ε_{22}^p in the direction of loading at a point in a typical selected grain is plotted in Fig. 1(a). It is evident that the deformation behaviour exhibits an oscillatory behaviour about a time-averaged or evolution of state variables. The frequency or rate of change of averaged variables is generally quite slow in comparison with the frequency of the applied cyclic loads. Consequently, it is conceivable to introduce two different time-scales in the solution of the governing equations of cyclic deformation in materials exhibiting crystal plasticity. The first corresponds to a

coarse or natural time-scale t that is characteristic of the long-term behaviour of the smooth averaged solution. The solution process for this time-scale can use time increments that are significantly longer than the period of a single cycle. The second is a fine time-scale τ that is necessary for providing adequate resolution to the rapidly varying behaviour of the evolving variables resulting from the periodic loading. The time increments in this scale, required for the solution of this behaviour, are considerably smaller than the period of the cycle.

The relation between the two time-scales t and τ may be defined as $t = \varepsilon\tau$, where $\varepsilon \ll 1$ is a small positive scaling parameter. A superscript ε associated with a variable denotes its association with both the time-scales. Consequently, all the response fields in the body $\phi^{(\varepsilon)}(\mathbf{x}, t)$ at a given spatial location \mathbf{x}

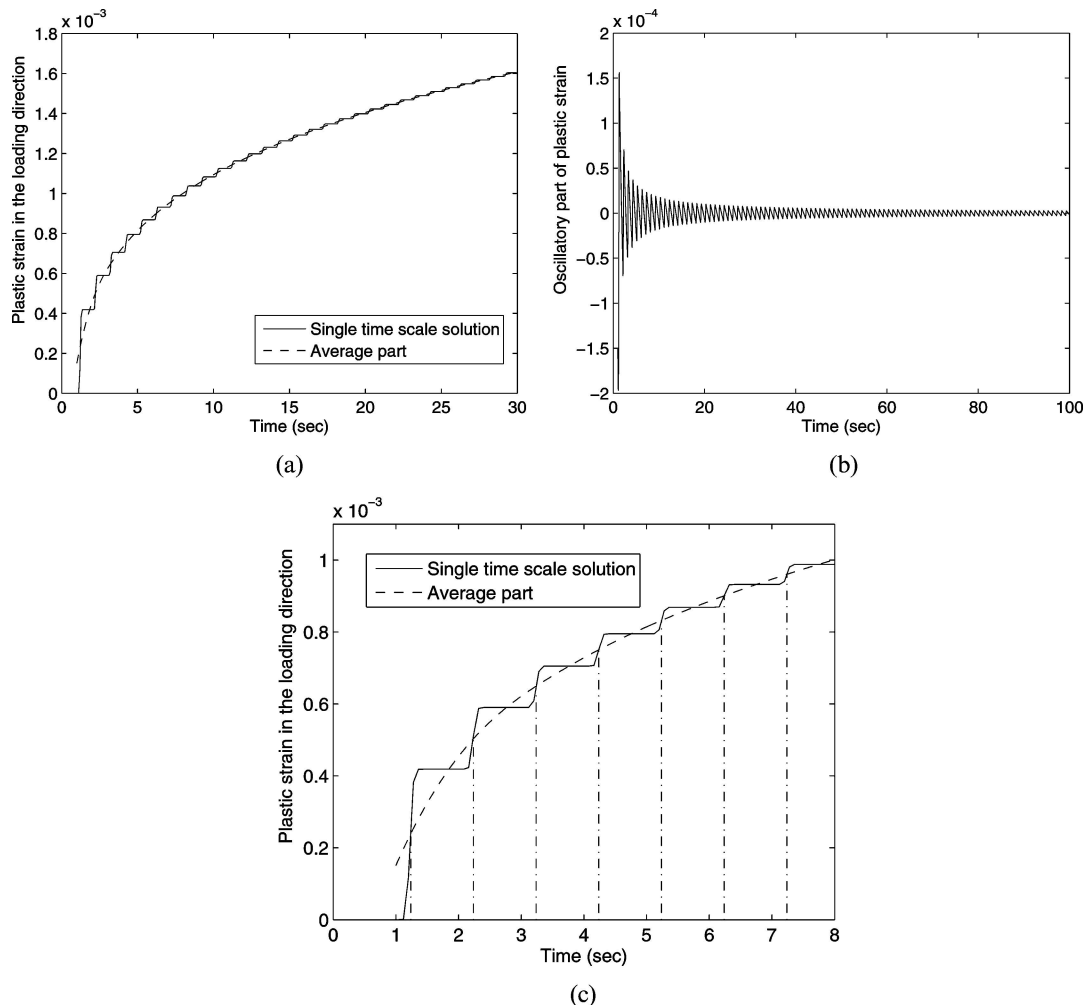


Fig. 1 The evolution of plastic strain with time at a point in the polycrystalline aggregate: (a) the exact and cycle-time-averaged plastic strain solution from a single-time integration algorithm; (b) the oscillatory part of the plastic strain solution; (c) the total and cycle-time averaged solution, showing the periodic nature of the intercept

are assumed to exhibit dependence on the coarse time-scale t and the fine time-scale τ and are expressed as

$$\phi^{(\varepsilon)}(\mathbf{x}, t) = \phi(\mathbf{x}, t, \tau) \tag{11}$$

Using the chain rule and the relation between the time-scales, the time derivatives in the two time-scales are given as

$$\dot{\phi}^{(\varepsilon)} = \frac{\partial \phi^{(\varepsilon)}}{\partial t} = \frac{\partial \phi}{\partial t} + \frac{1}{\varepsilon} \frac{\partial \phi}{\partial \tau} \tag{12}$$

where the overdot denotes the total derivative with time. It is implicit that all variables are functions of the position \mathbf{x} , and hence this will not be used explicitly below. The dashed line in Fig. 1(a) corresponds to the cycle-averaged value $\bar{\varepsilon}_{22}^p$ that is obtained by joining the time-averaged plastic strains in each cycle. The cycle-averaged field variable over a period T in the fine time-scale $\tau = t/\varepsilon$ at time t is defined as

$$\bar{\phi}(t) = \langle \phi(t, \tau) \rangle = \frac{1}{T} \int_{t/\varepsilon}^{1/\varepsilon + T} \phi(t, \tau) d\tau \tag{13}$$

The angle brackets $\langle \rangle$ correspond to the averaging operator. From Fig. 1(a) it is clear that cyclic oscillations are absent in the plot of $\bar{\varepsilon}_{22}^p$. A general decomposition of all variables in the constitutive equation is therefore proposed in the form

$$\phi(t, \tau) = \bar{\phi}(t) + \tilde{\phi}(t, \tau) \tag{14}$$

The overbar in equation (14) corresponds to the solution of a set of time-averaged equations. It should be noted that these solutions of the set of averaged governing equations might be different from the variables that are obtained by cycle averaging the single-time-scale solutions. The tilde, on the other hand, refers to the remainder of the solution (oscillatory portion). By definition of $\bar{\phi}(t)$ in equation (13), the following condition is obtained for the oscillator

$$\langle \tilde{\phi}(t, \tau) \rangle = 0 \tag{15}$$

Figure 1(b) is a plot of the oscillatory portion of the plastic strain $\tilde{\varepsilon}_{22}^p = \varepsilon_{22}^p - \bar{\varepsilon}_{22}^p$. It should be noted that the amplitude of the oscillations is a monotonic function of time, and the oscillations vary in both the t and the τ scales. From this example it is prudent

to assume that the non-periodic oscillatory part may be obtained by the superposition of a monotonically varying amplitude on a periodic cyclic response. Thus, the oscillatory portion is decomposed multiplicatively and additively as

$$\tilde{\phi}(t, \tau) = \tilde{\phi}^{\text{nos}}(t, \tau) \tilde{\phi}^{\text{per}}(\tau) = \tilde{\phi}^{\text{osc}}(t, \tau) + \tilde{\phi}^c(t) \tag{16}$$

The superscripts ‘nos’ and ‘per’ represent the monotonic and cyclic-periodic parts of the multiplicative decomposition respectively. The periodic portion of the response variables is expected to have the same frequency as that of the applied loading, while the monotonic part is induced by the evolving plasticity. An important characteristic of the oscillatory solution is deciphered from this multiplicative decomposition. Within each cycle, the relative location of the intercept of the solution with the time axis is periodic, i.e. the oscillator is zero at exactly the same cycle reference time $\hat{\tau} (\in [0, T])$ in each cycle. The oscillatory response is a direct consequence of the applied load. If the applied loading is aperiodic, it is reasonable to assume that only the zero intercept of the oscillator in any evolving variable is also periodic throughout the loading cycle. The condition does not require all oscillatory variables to have the same frequency. It only requires the relative position of the zero intercept in each cycle to remain the same. Thus, the total solution will intercept the average solution at the same cycle reference time $\hat{\tau}$ in each cycle, i.e.

$$\begin{aligned} \text{If } \tilde{\phi}(\hat{\tau}) = 0 \quad \text{for } \hat{\tau} \in [0, T] \quad \text{then} \\ \tilde{\phi}(n\hat{\tau}) = 0 \quad \forall n = 1, 2, 3, \dots \end{aligned} \tag{17}$$

This is depicted in Fig. 1(c). The initial conditions for the oscillatory solution in each cycle are posed by the relations (17). The additive decomposition in equation (16) is also necessary to create a link to the average solution, because of non-periodicity of the oscillator. The second term with a superscript ‘c’ corresponds to a compensator that arises from the definition of the averaged response. It is needed to annul the additional term in the average solution owing to the non-periodicity of the oscillatory part such that equation (15) can be satisfied.

Four independent variables are identified in the crystal plasticity based finite element equations:

- (a) the displacement field vector \mathbf{u} ;
- (b) the plastic deformation gradient tensor \mathbf{F}^p ;
- (c) the slip system resistance parameter g^{α} ;
- (d) scalar kinematic variable Ω^{α} .

Following equations (14) and (16), these four independent variables can be decomposed as

$$\begin{aligned}
 u_i^\varepsilon(t) &= u_i(t, \tau) = \bar{u}_i(t) + \tilde{u}_i^{\text{osc}}(t, \tau) + \tilde{u}_i^c(t) \\
 (F^{\text{p}})_{ij}^\varepsilon(t) &= (F^{\text{p}})_{ij}(t, \tau) \\
 &= (\bar{F}^{\text{p}})_{ij}(t) + (\tilde{F}^{\text{p}})_{ij}^{\text{osc}}(t, \tau) + (\tilde{F}^{\text{p}})_{ij}^c(t) \\
 (g^\alpha)^\varepsilon(t) &= (g^\alpha)(t, \tau)(\bar{g}^\alpha)(t) + (\tilde{g}^\alpha)^{\text{osc}}(t, \tau) + (\tilde{g}^\alpha)^c(t) \\
 (\Omega^\alpha)^\varepsilon(t) &= (\Omega^\alpha)(t, \tau) \\
 &= (\bar{\Omega}^\alpha)(t) + (\tilde{\Omega}^\alpha)^{\text{osc}}(t, \tau) + (\tilde{\Omega}^\alpha)^c(t)
 \end{aligned} \tag{18}$$

3.1 Asymptotic expansion of the oscillatory solution

From the characteristics exhibited by the oscillatory solution in Fig. 1(b), the oscillator $\tilde{\phi}(t, \tau)$ can be expanded into an asymptotic series as

$$\tilde{\phi}^{(\varepsilon)}(t, \tau) = \tilde{\phi}^{(0)}(t, \tau) + \varepsilon \tilde{\phi}^{(1)}(t, \tau) + \varepsilon^2 \tilde{\phi}^{(2)}(t, \tau) + o(\varepsilon^3) \tag{19}$$

Since the oscillator has to satisfy condition (15) for any arbitrary ε , each term in the asymptotic expansion in equation (19) has individually to satisfy condition (15). Substitution of equation (16) into equation (19) results in

$$\begin{aligned}
 \tilde{\phi}^{(\varepsilon)}(t, \tau) &= [\tilde{\phi}^{\text{osc}(0)}(t, \tau) + \tilde{\phi}^{\text{c}(0)}(t)] \\
 &+ \varepsilon [\tilde{\phi}^{\text{osc}(1)}(t, \tau) + \tilde{\phi}^{\text{c}(1)}(t)] \\
 &+ \varepsilon^2 [\tilde{\phi}^{\text{osc}(2)}(t, \tau) + \tilde{\phi}^{\text{c}(2)}(t)] + o(\varepsilon^3)
 \end{aligned} \tag{20}$$

Thus, any field variable $\phi(t, \tau)$ can be expanded as

$$\begin{aligned}
 \phi^{(\varepsilon)}(t, \tau) &= \underbrace{\bar{\phi}(t) + [\tilde{\phi}^{\text{osc}(0)}(t, \tau) + \tilde{\phi}^{\text{c}(0)}(t)]}_{\phi^{(0)}} \\
 &+ \varepsilon \underbrace{[\tilde{\phi}^{\text{osc}(1)}(t, \tau) + \tilde{\phi}^{\text{c}(1)}(t)]}_{\phi^{(1)}} \\
 &+ \varepsilon^2 \underbrace{[\tilde{\phi}^{\text{osc}(2)}(t, \tau) + \tilde{\phi}^{\text{c}(2)}(t)]}_{\phi^{(2)}} + o(\varepsilon^3)
 \end{aligned} \tag{21}$$

Remark

The terms in equation (21) have the following characteristics.

1. The time-averaged response $\bar{\phi}(t)$ is assumed to be a function of t alone, and coarse-time-scale computations using averaged laws are used in determining their evolution. Consequently, the derivatives $[\partial \bar{\phi}(t)] / \partial \tau = 0$.

2. The oscillatory part of the remaining portion $\tilde{\phi}^{\text{osc}}$ of the solution is a function of both t and τ . Asymptotic expansions of these variables in the τ scale may be assumed about the coarse scale-time t .
3. Finally, the compensatory term $\tilde{\phi}^c$ is a function of t only, and thus $[\partial \tilde{\phi}^c(t)] / \partial \tau = 0$. Since this term arises from averaging the oscillatory term, asymptotic expansions of these variables may be assumed about t in the t time-scale itself.

The independent variables in the crystal plasticity FE model may then be expanded as

$$\begin{aligned}
 u_i^\varepsilon(t) &= \bar{u}_i(t) + [\tilde{u}_i^{\text{osc}(0)}(t, \tau) + \tilde{u}_i^{\text{c}(0)}(t)] \\
 &+ \varepsilon [\tilde{u}_i^{\text{osc}(1)}(t, \tau) + \tilde{u}_i^{\text{c}(1)}(t)] + \dots \\
 (F^{\text{p}})_{ij}^\varepsilon(t) &= (\bar{F}^{\text{p}})_{ij}(t) + [(\tilde{F}^{\text{p}})_{ij}^{\text{osc}(0)}(t, \tau) + (\tilde{F}^{\text{p}})_{ij}^{\text{c}(0)}(t)] \\
 &+ \varepsilon [(\tilde{F}^{\text{p}})_{ij}^{\text{osc}(1)}(t, \tau) + (\tilde{F}^{\text{p}})_{ij}^{\text{c}(1)}(t)] + \dots \\
 (g^\alpha)^\varepsilon(t) &= (\bar{g}^\alpha)(t) + [(\tilde{g}^\alpha)^{\text{osc}(0)}(t, \tau) + (\tilde{g}^\alpha)^{\text{c}(0)}(t)] \\
 &+ \varepsilon [(\tilde{g}^\alpha)^{\text{osc}(1)}(t, \tau) + (\tilde{g}^\alpha)^{\text{c}(1)}(t)] + \dots \\
 (\Omega^\alpha)^\varepsilon(t) &= (\bar{\Omega}^\alpha)(t) + [(\tilde{\Omega}^\alpha)^{\text{osc}(0)}(t, \tau) + (\tilde{\Omega}^\alpha)^{\text{c}(0)}(t)] \\
 &+ \varepsilon [(\tilde{\Omega}^\alpha)^{\text{osc}(1)}(t, \tau) + (\tilde{\Omega}^\alpha)^{\text{c}(1)}(t)] + \dots
 \end{aligned} \tag{22}$$

The time derivatives of these independent variables, $\phi^{(\varepsilon)}(t)$, are expressed by substituting equation (21) into (12) as

$$\begin{aligned}
 \dot{\phi}^{(\varepsilon)}(t) &= \frac{1}{\varepsilon} \frac{\partial}{\partial \tau} [\bar{\phi}(t) + \tilde{\phi}^{\text{osc}(0)}(t, \tau) + \tilde{\phi}^{\text{c}(0)}(t)] \\
 &+ \left\{ \frac{\partial}{\partial t} [\bar{\phi}(t) + \tilde{\phi}^{\text{osc}(0)}(t, \tau) + \tilde{\phi}^{\text{c}(0)}(t)] \right. \\
 &\quad \left. + \frac{\partial}{\partial \tau} [\tilde{\phi}^{\text{osc}(1)}(t, \tau) + \tilde{\phi}^{\text{c}(1)}(t)] \right\} \\
 &+ \varepsilon \left\{ \frac{\partial}{\partial t} [\tilde{\phi}^{\text{osc}(1)}(t, \tau) + \tilde{\phi}^{\text{c}(1)}(t)] \right. \\
 &\quad \left. + \frac{\partial}{\partial \tau} [\tilde{\phi}^{\text{osc}(2)}(t, \tau) + \tilde{\phi}^{\text{c}(2)}(t)] \right\} + o(\varepsilon^2)
 \end{aligned} \tag{23}$$

Since $[\partial\bar{\phi}(t)]/\partial\tau = 0$ and $[\partial\tilde{\phi}^c(t)]/\partial\tau = 0$, equation (23) reduces to

$$\begin{aligned} \phi^{(\varepsilon)}(t) = & \frac{1}{\varepsilon} \left[\frac{\partial\tilde{\phi}^{\text{nos}(0)}(t, \tau)}{\partial\tau} \right] \\ & + \left[\frac{\partial\bar{\phi}(t)}{\partial t} + \frac{\partial\tilde{\phi}^{\text{osc}(0)}(t, \tau)}{\partial t} + \frac{\partial\tilde{\phi}^{\text{c}(0)}(t)}{\partial t} \right. \\ & \quad \left. + \frac{\partial\tilde{\phi}^{\text{osc}(0)}(t, \tau)}{\partial\tau} \right] \\ & + \sum_{n=1,2,\dots} \varepsilon^n \left[\frac{\partial\tilde{\phi}^{\text{osc}(n)}(t, \tau)}{\partial t} + \frac{\partial\tilde{\phi}^{\text{c}(n)}(t)}{\partial t} \right. \\ & \quad \left. + \frac{\partial\tilde{\phi}^{\text{nos}(n+1)}(t, \tau)}{\partial\tau} \right] \end{aligned} \quad (24)$$

The time derivatives of the independent variables in equation (22) then become

$$\begin{aligned} (\dot{F}^{\text{p}})^{\varepsilon}_{ij}(t) = & \frac{1}{\varepsilon} \left[\frac{\partial(\tilde{F}^{\text{p}})^{\text{osc}(0)}}{\partial\tau} \right] \\ & + \left[\frac{\partial(\bar{F}^{\text{p}})_{ij}}{\partial t} + \frac{\partial(\tilde{F}^{\text{p}})^{\text{osc}(0)}}{\partial t} + \frac{\partial(\tilde{F}^{\text{p}})^{\text{c}(0)}}{\partial t} \right. \\ & \quad \left. + \frac{\partial(\tilde{F}^{\text{p}})^{\text{osc}(0)}}{\partial\tau} \right] + \dots \\ (\dot{g}^{\alpha})^{\varepsilon}(t) = & \frac{1}{\varepsilon} \left[\frac{\partial(\tilde{g}^{\alpha})^{\text{osc}(0)}}{\partial\tau} \right] \\ & + \left[\frac{\partial\bar{g}^{\alpha}}{\partial t} + \frac{\partial(\tilde{g}^{\alpha})^{\text{osc}(0)}}{\partial t} + \frac{\partial(\tilde{g}^{\alpha})^{\text{c}(0)}}{\partial t} \right. \\ & \quad \left. + \frac{\partial(\tilde{g}^{\alpha})^{\text{osc}(0)}}{\partial\tau} \right] + \dots \\ (\dot{\Omega}^{\alpha})^{\varepsilon}(t) = & \frac{1}{\varepsilon} \left[\frac{\partial(\tilde{\Omega}^{\alpha})^{\text{osc}(0)}}{\partial\tau} \right] \\ & + \left[\frac{\partial\bar{\Omega}^{\alpha}}{\partial t} + \frac{\partial(\tilde{\Omega}^{\alpha})^{\text{osc}(0)}}{\partial t} + \frac{\partial(\tilde{\Omega}^{\alpha})^{\text{c}(0)}}{\partial t} \right. \\ & \quad \left. + \frac{\partial(\tilde{\Omega}^{\alpha})^{\text{osc}(0)}}{\partial\tau} \right] + \dots \end{aligned} \quad (25)$$

3.2 Expressions for the dependent variables in crystal plasticity

The average part and different orders of the oscillatory parts of the dependent variables in the crystal plasticity equations are derived by substituting the

expansions of primary variables (22) into equations (1) to (10). The deformation gradient $F^{\text{e}}_{ij}(t, \tau)$ is expressed as

$$F^{\text{e}}_{ij}(t, \tau) = \underbrace{\bar{u}_{i,j}(t)}_{F_{ij}(t)} + \delta_{ij} + \underbrace{\tilde{u}_{i,j}^{(0)}(t, \tau)}_{\bar{F}_{ij}^{(0)}(t, \tau)} + \varepsilon \underbrace{\tilde{u}_{i,j}^{(1)}(t, \tau)}_{\bar{F}_{ij}^{(1)}(t, \tau)} + o(\varepsilon^2) \quad (26)$$

The averaged and the zero- and first-order terms in the asymptotic expansion of the oscillator are calculated for various important evolving variables. For example, these terms for the inverse of the plastic deformation gradient $F^{\text{p}(e)-1}$ are

Average:

$$\bar{F}^{\text{p}-1} = [\bar{F}^{\text{p}}]^{-1}$$

Oscillator $o(\varepsilon^0)$:

$$\tilde{F}^{\text{p}-1(0)} = [\tilde{F}^{\text{p}(0)}]^{-1}$$

Oscillator $o(\varepsilon^1)$:

$$\tilde{F}^{\text{p}-1(1)} = -(\bar{F}^{\text{p}} + \tilde{F}^{\text{p}(0)})^{-1} \tilde{F}^{\text{p}(1)} (\bar{F}^{\text{p}} + \tilde{F}^{\text{p}(0)})^{-1} \quad (27)$$

Similarly, the terms for the elastic deformation gradient $F^{\text{e}(e)}$, the elastic Lagrange–Green strain $E^{\text{e}(e)}$, the second Piola–Kirchhoff stress $S^{\text{e}(e)}$, and the resolved shear stress $\tau^{\alpha(e)}$ are expressed as follows

For $F^{\text{e}(e)}$

Average:

$$\bar{F}^{\text{e}} = \bar{F}^{\text{e}} \bar{F}^{\text{p}-1} + \langle \tilde{F}^{(0)} \tilde{F}^{\text{p}-1(0)} \rangle$$

Oscillator $o(\varepsilon^0)$:

$$\tilde{F}^{\text{e}(0)} = \tilde{F}^{(0)} (\bar{F}^{\text{p}-1} + \tilde{F}^{\text{p}-1(0)}) + \bar{F}^{\text{e}} \tilde{F}^{\text{p}-1(0)}$$

Oscillator $o(\varepsilon^1)$:

$$\tilde{F}^{\text{e}(1)} = \tilde{F}^{(1)} (\bar{F}^{\text{p}-1} + \tilde{F}^{\text{p}-1(0)}) + (\bar{F}^{\text{e}} + \tilde{F}^{(0)}) \tilde{F}^{\text{p}-1(0)} \quad (28)$$

For $E^{\text{e}(e)}$

Average:

$$\bar{E}^{\text{e}} \approx \frac{1}{2} (\bar{F}^{\text{e}} \bar{F}^{\text{e}} - \delta_{ij})$$

Oscillator $o(\varepsilon^0)$:

$$\tilde{E}^{\text{e}(0)} = \frac{1}{2} (\tilde{F}^{\text{e}(0)} \bar{F}^{\text{e}} + \bar{F}^{\text{e}} \tilde{F}^{\text{e}(0)} + \tilde{F}^{\text{e}(0)} \tilde{F}^{\text{e}(0)})$$

Oscillator $o(\varepsilon^1)$:

$$\tilde{E}^{\text{e}(1)} = \frac{1}{2} [\tilde{F}^{\text{e}(1)} (\bar{F}^{\text{e}} + \tilde{F}^{\text{e}(0)}) + (\bar{F}^{\text{e}} + \tilde{F}^{\text{e}(0)}) \tilde{F}^{\text{e}(1)}] \quad (29)$$

For $S_{ij}^{(\varepsilon)}$

Average:

$$\bar{S}_{ij} = C_{ijkl} \bar{E}_{kl}^e$$

Oscillator $o(\varepsilon^0)$:

$$\tilde{S}_{ij}^{(0)} = C_{ijkl} \tilde{E}_{kl}^{e(0)}$$

Oscillator $o(\varepsilon^1)$:

$$\tilde{S}_{ij}^{(1)} = C_{ijkl} \tilde{E}_{kl}^{e(1)} \quad (30)$$

For $\tau^{\alpha(\varepsilon)}$

Average:

$$\bar{\tau}^{\alpha} \approx \bar{F}_{ki}^e \bar{F}_{km}^e \bar{S}_{mj}^{\alpha}$$

Oscillator $o(\varepsilon^0)$:

$$\tilde{\tau}^{\alpha(0)} \approx F_{ki}^{e(0)} F_{km}^{e(0)} \tilde{S}_{mj}^{\alpha(0)}$$

Oscillator $o(\varepsilon^1)$:

$$\tilde{\tau}^{\alpha(1)} \approx F_{ki}^{e(0)} F_{km}^{e(0)} \tilde{S}_{mj}^{\alpha(1)} \quad (31)$$

For $\sigma_{kin\ ij}^{(\varepsilon)}$ and $\tau_{kin}^{\alpha(\varepsilon)}$

Average:

$$\bar{\sigma}_{kin\ ij} = \sum_{\alpha} \bar{\Omega}^{\alpha} (m_i^{\alpha} n_j^{\alpha} + m_j^{\alpha} n_i^{\alpha})$$

$$\bar{\tau}_{kin}^{\alpha} = \bar{\sigma}_{kin\ ij} m_i^{\alpha} n_j^{\alpha}$$

Oscillator $o(\varepsilon^0)$:

$$\tilde{\sigma}_{kin\ ij}^{(0)} = \sum_{\alpha} \tilde{\Omega}^{\alpha(0)} (m_i^{\alpha} n_j^{\alpha} + m_j^{\alpha} n_i^{\alpha})$$

$$\tilde{\tau}_{kin}^{\alpha(0)} = \tilde{\sigma}_{kin\ ij}^{(0)} m_i^{\alpha} n_j^{\alpha}$$

Oscillator $o(\varepsilon^1)$:

$$\tilde{\sigma}_{kin\ ij}^{(1)} = \sum_{\alpha} \tilde{\Omega}^{\alpha(1)} (m_i^{\alpha} n_j^{\alpha} + m_j^{\alpha} n_i^{\alpha})$$

$$\tilde{\tau}_{kin}^{\alpha(1)} = \tilde{\sigma}_{kin\ ij}^{(1)} m_i^{\alpha} n_j^{\alpha} \quad (32)$$

The averaged and the oscillator terms are coupled for a few variables, such as the rate of evolution of shear slip $\dot{\gamma}^{\alpha(\varepsilon)}$, the rate of evolution of hardness variables, etc. Thus

For $\dot{\gamma}^{\alpha(\varepsilon)}$

Average and oscillator $o(\varepsilon^0)$:

$$\bar{\dot{\gamma}}^{\alpha} + \dot{\gamma}^{\alpha(0)} = \left| \frac{\bar{\tau}_{\text{eff}}^{\alpha} + \tilde{\tau}_{\text{eff}}^{\alpha(0)}}{\bar{g}^{\alpha} + \tilde{g}^{\alpha(0)}} \right|^{1/m-1} \left(\frac{\bar{\tau}_{\text{eff}}^{\alpha} + \tilde{\tau}_{\text{eff}}^{\alpha(0)}}{\bar{g}^{\alpha} + \tilde{g}^{\alpha(0)}} \right)$$

Oscillator $o(\varepsilon^1)$:

$$\begin{aligned} \dot{\gamma}^{\alpha(1)} = & \left| \frac{\bar{\tau}_{\text{eff}}^{\alpha} + \tilde{\tau}_{\text{eff}}^{\alpha(0)}}{\bar{g}^{\alpha} + \tilde{g}^{\alpha(0)}} \right|^{1/m-1} \left(\frac{\bar{\tau}_{\text{eff}}^{\alpha} + \tilde{\tau}_{\text{eff}}^{\alpha(0)}}{\bar{g}^{\alpha} + \tilde{g}^{\alpha(0)}} \right) \\ & \times \left\{ \frac{1}{m} \left(\frac{\tau_{\text{eff}}^{\alpha(1)}}{\bar{\tau}_{\text{eff}}^{\alpha} + \tilde{\tau}_{\text{eff}}^{\alpha(0)}} - \frac{\tilde{g}^{\alpha(1)}}{\bar{g}^{\alpha} + \tilde{g}^{\alpha(0)}} \right) \right\} \quad (33) \end{aligned}$$

For $\dot{g}^{\alpha(\varepsilon)}$

Average and oscillator $o(\varepsilon^0)$:

$$\bar{\dot{g}}^{\alpha} + \dot{g}^{\alpha(0)} = \sum_{\beta}^{n\text{slip}} (\bar{h}^{\alpha\beta} + \tilde{h}^{\alpha\beta(0)}) |\dot{\gamma}^{\beta} + \dot{\gamma}^{\beta(0)}|$$

Oscillator $o(\varepsilon^1)$:

$$\dot{g}^{\alpha(1)} = \sum_{\beta}^{n\text{slip}} (\bar{h}^{\alpha\beta} + \tilde{h}^{\alpha\beta(0)}) |\dot{\gamma}^{\beta(1)}| + \sum_{\beta}^{n\text{slip}} \tilde{h}^{\alpha\beta(1)} |\dot{\gamma}^{\beta} + \dot{\gamma}^{\beta(0)}| \quad (34)$$

For $\dot{\Omega}^{\alpha(\varepsilon)}$

Average and oscillator $o(\varepsilon_0)$:

$$\bar{\dot{\Omega}}^{\alpha} + \dot{\Omega}^{\alpha(0)} = c(\dot{\gamma}^{\alpha} + \dot{\gamma}^{\alpha(0)}) - d(\bar{\Omega}^{\alpha} + \tilde{\Omega}^{\alpha(0)}) |\dot{\gamma}^{\alpha} + \dot{\gamma}^{\alpha(0)}|$$

Oscillator $o(\varepsilon^1)$:

$$\dot{\Omega}^{\alpha(1)} = c\dot{\gamma}^{\alpha(1)} - d(\bar{\Omega}^{\alpha} + \tilde{\Omega}^{\alpha(0)}) |\dot{\gamma}^{\alpha(1)}| - d\tilde{\Omega}^{\alpha(1)} |\dot{\gamma}^{\alpha} + \dot{\gamma}^{\alpha(0)}| \quad (35)$$

The decomposed expressions of the constitutive variables are now substituted into the governing equations of the original initial boundary-value problem to obtain an average problem and oscillatory problems.

3.3 Decomposition of the governing equations

The various evolution equations (equations (25) to (35)) are then substituted into the governing equilibrium and constitutive equations to obtain different sets of initial boundary-value problems of the polycrystalline material subjected to cyclic loading. The average and each order of the oscillatory problem are obtained as a result of averaging the equations and separating terms with different exponents of ε , i.e. ε^{-1} , ε^0 , etc. The resulting equations are summarized next.

3.3.1 Averaged problem

The average initial boundary-value problem can be summarized as

Equilibrium:

$$\bar{\alpha}_{i,j,j} + \bar{b}_i = 0$$

BCs:

$$\bar{\sigma}_{ij} n_j = \langle t_i^* \rangle \quad \text{on } \Gamma_t, \quad \bar{u}_i = \langle u_i^* \rangle \quad \text{on } \Gamma_u$$

ICs:

$$\bar{\gamma}^{\alpha} = \langle \gamma^{\alpha} \rangle_{\text{cyc}_n}, \quad \bar{g}^{\alpha} = \langle g^{\alpha} \rangle_{\text{cyc}_n}$$

$$\bar{\Omega}^{\alpha} = \langle \Omega^{\alpha} \rangle_{\text{cyc}_n}$$

where n is the cycle number from which the average solution begins

Constitutive relations:

$$\begin{aligned}\bar{F}_{ij} &= \bar{F}_{ik}^e \bar{F}_{kj}^p{}^{-1} \\ \bar{E}_{ij}^e &= \frac{1}{2} (\bar{F}_{ki}^e \bar{F}_{kj}^e - \delta_{ij}) \\ \bar{S}_{ij} &= C_{ijkl} \bar{E}_{kl}^e \\ \dot{\bar{F}}_{ik}^p \bar{F}_{kj}^p{}^{-1} &= \sum_{\alpha}^{nslip} \dot{\gamma}^{\alpha} s_{ij}^{\alpha} \quad (36)\end{aligned}$$

together with the evolution of plastic variables $\bar{\gamma}^{\alpha}$, \bar{g}^{α} , and $\bar{\Omega}^{\alpha}$. Comparing the independent coefficients of ε^0 in the evolution equations (equations (25) to (35)) results in the evolution equations for plastic variables for the average problem, as summarized below

Shear strain rate S :

$$\dot{\gamma}^{\alpha(0)} = \dot{\gamma}^{\alpha(0)} + \dot{\gamma}^{\alpha(0)} = \dot{\gamma}_0 \left| \frac{\bar{\tau}_{eff}^{\alpha} + \bar{\tau}_{eff}^{\alpha(0)}}{\bar{g}^{\alpha}} \right|^{1/m-1} \left(\frac{\bar{\tau}_{eff}^{\alpha} + \bar{\tau}_{eff}^{\alpha(0)}}{\bar{g}^{\alpha}} \right)$$

Flow rule F :

$$\begin{aligned}\frac{\partial(\bar{F}^p)_{ij}}{\partial t} + \frac{\partial(\bar{F}^p)_{ij}^{osc(0)}}{\partial t} + \frac{\partial(\bar{F}^p)_{ij}^{c(0)}}{\partial t} + \frac{\partial(\bar{F}^p)^{nos(1)}}{\partial \tau} \\ = \sum_{\alpha=1}^{nslip} \dot{\gamma}^{\alpha(0)} s_{ik}^{\alpha} F_{kj}^{p(0)} \\ \Rightarrow \frac{\partial(\bar{F}^p)_{ij}}{\partial t} + \frac{\partial(\bar{F}^p)^{osc(1)}}{\partial \tau} = \sum_{\alpha=1}^{nslip} \dot{\gamma}^{\alpha(0)} s_{ik}^{\alpha} \bar{F}_{kj}^p, \\ \text{since } \frac{\partial(\bar{F}^p)_{ij}^{osc(0)}}{\partial t} = \frac{\partial(\bar{F}^p)_{ij}^{c(0)}}{\partial t} = \bar{F}_{ij}^{p(0)} = 0\end{aligned}$$

Hardening evolution H :

$$\begin{aligned}\frac{\partial \bar{g}^{\alpha}}{\partial t} + \frac{\partial(\bar{g}^{\alpha})^{osc(0)}}{\partial t} + \frac{\partial(\bar{g}^{\alpha})^{c(0)}}{\partial t} + \frac{\partial(\bar{g}^{\alpha})^{osc(0)}}{\partial \tau} \\ = \sum_{\beta=1}^{nslip} h^{\alpha\beta(0)} |\dot{\gamma}|^{\beta(0)} \\ \Rightarrow \frac{\partial \bar{g}^{\alpha}}{\partial t} + \frac{\partial(\bar{g}^{\alpha})^{osc(1)}}{\partial \tau} = \sum_{\beta=1}^{nslip} (\bar{h}^{\alpha\beta} + \bar{h}^{\alpha\beta(0)}) |\dot{\gamma} + \dot{\gamma}^{(0)}|^{\beta} \\ \text{since } \frac{\partial(\bar{g}^{\alpha})^{osc(0)}}{\partial t} = \frac{\partial(\bar{g}^{\alpha})^{c(0)}}{\partial t} = \bar{g}^{\alpha(0)} = 0\end{aligned}$$

Back stress evolution B :

$$\begin{aligned}\frac{\partial \bar{\Omega}^{\alpha}}{\partial t} + (\bar{\Omega}^{\alpha})^{per} \frac{\partial(\bar{\Omega}^{\alpha})^{osc(0)}}{\partial t} + \frac{\partial(\bar{\Omega}^{\alpha})^{c(0)}}{\partial t} + \frac{\partial(\bar{\Omega}^{\alpha})^{osc(1)}}{\partial \tau} \\ = c \dot{\gamma}^{\alpha(0)} - d \Omega^{\alpha(0)} |\dot{\gamma}|^{\alpha(0)} \\ \Rightarrow \frac{\partial \bar{\Omega}^{\alpha}}{\partial t} + \frac{\partial(\bar{\Omega}^{\alpha})^{osc(1)}}{\partial \tau} = c (\dot{\gamma} + \dot{\gamma}^{(0)})^{\alpha} - d \bar{\Omega}^{\alpha} |\dot{\gamma} + \dot{\gamma}^{(0)}|^{\alpha} \\ \text{since } \frac{\partial(\bar{\Omega}^{\alpha})^{osc(0)}}{\partial t} = \frac{\partial(\bar{\Omega}^{\alpha})^{c(0)}}{\partial t} = \bar{\Omega}^{\alpha(0)} = 0 \quad (37)\end{aligned}$$

Remarks

Evolution equations (37) are coupled, i.e. the rate of evolution of average variables is dependent upon both the average and the oscillatory variables, and vice versa. This requires having to solve the oscillatory problem to obtain the averaged variables, and consequently simultaneous computations are needed for the two time-scales. Such computing can be prohibitive and diminishes the advantage of the overall approach. To overcome this shortcoming, it is necessary to decouple equations (37) to define $\dot{\gamma}^{\alpha}$, \dot{g}^{α} , and $\dot{\Omega}^{\alpha}$ such that the average problem with time increments much greater than the time period of the applied loading can be solved without solving the oscillatory problems. A decoupling algorithm that can operate on equations (37) to yield a set of independent averaged equations for the initial boundary-value problem is proposed in section 4 through the introduction of some special assumptions.

3.3.2 Oscillatory equations: zero order

Isolating the coefficients of ε^{-1} in the evolution equations (equations (25) to (35)) results in the zero-order equations for plastic variables in the oscillatory problem. They are

Flow rule F :

$$\frac{\partial(\bar{F}^p)_{ij}^{osc(0)}}{\partial \tau} = \sum_{\alpha}^{nslip} \dot{\gamma}^{\alpha(-1)} s_{ik}^{\alpha} F_{kj}^{p(0)} = 0$$

Hardening evolution H :

$$\frac{\partial(\bar{g}^{\alpha})^{osc(0)}}{\partial \tau} = 0$$

Back stress evolution B :

$$\frac{\partial(\bar{\Omega}^{\alpha})^{osc(0)}}{\partial \tau} = 0 \quad (38)$$

Important inferences can be drawn from equations (38).

1. Zero-order terms of the oscillatory plastic variables may be assumed to be zero without any loss of generality, i.e.

$$(\bar{F}^p)_{ij}^{osc(0)} = 0, \quad (\bar{g}^{\alpha})^{osc(0)} = 0, \quad (\bar{\Omega}^{\alpha})^{osc(0)} = 0$$

2. Since the compensatory terms are consequences of averaging the above terms, their corresponding zero-order components are also zero

$$(\bar{F}^p)_{ij}^{c(0)} = 0, \quad (\bar{g}^{\alpha})^{c(0)} = 0, \quad (\bar{\Omega}^{\alpha})^{c(0)} = 0$$

Thus, the zero-order oscillatory initial boundary-value problem can be summarized as

Equilibrium:

$$\tilde{\sigma}_{ij,j}^{(0)} + \tilde{b}_i^{(0)} = 0$$

BCs:

$$\tilde{\sigma}_{ij}^{(0)} n_j = t_i^* - \langle t_i^* \rangle \quad \text{on } \Gamma_t, \quad \tilde{u}_i^{(0)} = u_i^* - \langle u_i^* \rangle \quad \text{on } \Gamma_u$$

Constitutive relations:

$$\begin{aligned} \tilde{F}_{ij}^{e(0)} &= \tilde{F}_{ik}^{(0)} \tilde{F}_{kj}^{p-1} \\ \tilde{E}_{ij}^{e(0)} &= \frac{1}{2} (\tilde{F}_{ki}^e \tilde{F}_{kj}^{e(0)} + \tilde{F}_{ki}^{e(0)} \tilde{F}_{kj}^e + \tilde{F}_{ki}^{e(0)} \tilde{F}_{kj}^{e(0)}) \\ \tilde{S}_{ij}^{(0)} &= C_{ijkl} \tilde{E}_{kl}^{e(0)} \end{aligned} \quad (39)$$

3.4 Oscillatory equations: first order

The first-order oscillators can be solved using the averaged and the zero-order oscillators from the following equations

Shear strain rate S :

$$\dot{\gamma}^{\alpha(0)} = \dot{\gamma}_0 \left| \frac{\bar{\tau}_{\text{eff}}^\alpha + \tilde{\tau}_{\text{eff}}^{\alpha(0)}}{\bar{g}^\alpha + \tilde{g}^{\alpha(0)}} \right|^{1/m-1} \left(\frac{\bar{\tau}_{\text{eff}}^\alpha + \tilde{\tau}_{\text{eff}}^{\alpha(0)}}{\bar{g}^\alpha + \tilde{g}^{\alpha(0)}} \right) - \dot{\gamma}^\alpha$$

Flow rule F :

$$\frac{\partial (\tilde{F}^p)^{\text{osc}(1)}}{\partial \tau} = \sum_{\alpha=1}^{n_{\text{slip}}} \dot{\gamma}^{\alpha(0)} s_{ik}^\alpha (\tilde{F}_{kj}^p + \tilde{F}_{kj}^{p(0)}) - \frac{\partial (\tilde{F}^p)_{ij}}{\partial t}$$

Hardening evolution H :

$$\frac{\partial (\tilde{g}^\alpha)^{\text{osc}(1)}}{\partial \tau} = \sum_{\beta=1}^{n_{\text{slip}}} (\bar{h}^{\alpha\beta} + \tilde{h}^{\alpha\beta(0)}) |\dot{\gamma} + \dot{\gamma}^{(0)}|^\beta - \frac{\partial \bar{g}^\alpha}{\partial t}$$

Back stress evolution B :

$$\begin{aligned} \frac{\partial (\tilde{\Omega}^\alpha)^{\text{nos}(1)}}{\partial \tau} &= c(\dot{\gamma} + \dot{\gamma}^{(0)})^\alpha \\ &- d(\bar{\Omega}^\alpha + \tilde{\Omega}^{\alpha(0)}) |\dot{\gamma} + \dot{\gamma}^{(0)}|^\alpha - \frac{\partial \bar{\Omega}^\alpha}{\partial t} \end{aligned} \quad (40)$$

The τ -scale dependent oscillator terms are solved by an implicit time integration scheme based on the backward Euler method. Following the evaluation of $(\tilde{F}^p)_{ij}^{\text{osc}(1)}$, $(\tilde{g}^\alpha)^{\text{osc}(1)}$, and $(\tilde{\Omega}^\alpha)^{\text{osc}(1)}$, the corresponding compensatory terms can be obtained from the conditions

$$\begin{aligned} \frac{1}{T} \int_t^{t+nT} [(\tilde{F}^p)_{ij}^{\text{osc}(1)} + (\tilde{F}^p)_{ij}^{c(1)}] d\tau &= 0 \\ \frac{1}{T} \int_t^{t+nT} [(\tilde{g}^\alpha)^{\text{osc}(1)} + (\tilde{g}^\alpha)^{c(1)}] d\tau &= 0 \\ \frac{1}{T} \int_t^{t+nT} [(\tilde{\Omega}^\alpha)^{\text{osc}(1)} + (\tilde{\Omega}^\alpha)^{c(1)}] d\tau &= 0 \end{aligned} \quad (41)$$

where n is the number of cycles considered in the averaging process. This study considers only up

to first-order terms in the asymptotic expansion. However, it is possible to add higher-order terms in the asymptotic expansion on the basis of oscillatory solutions of the crystal plasticity variables in a similar manner.

4 CYCLE-AVERAGED EFFECTIVE CONSTITUTIVE EQUATIONS

The coupled evolution equations (37) cause coupling between the averaged and the oscillatory problems. If all the response fields are assumed to be locally periodic in τ , the averaged and the oscillatory problems can be decoupled by applying the averaging operator $\langle \cdot \rangle$ to the coupled evolution equations. However, the periodic assumption made in reference [23] is not valid in the case of evolving plastic variables. A near-periodic assumption is made in reference [24] for decoupling variables in two time-scales. However, this formulation results in a coupled oscillatory and averaged problem, where the oscillatory solution with small time increments has to be solved simultaneously with a staggered averaged solution. This coupling makes the method computationally prohibitive for simulations with a large number of cycles. In the present work, a decoupling scheme that does not depend on periodicity assumptions and can result in a high computational efficiency is proposed. The method is of considerable practical interest for analysis of cyclic deformation leading to fatigue.

Sets of time-scale or cycle-averaged constitutive equations are developed such that the averaged problem is totally decoupled from the oscillatory problem. An averaged function $\bar{\phi}(t)$ can be interpreted as a function that is the result of continuous representation of a set of data points $\bar{\phi}(n)$ obtained from detailed single-scale simulation, i.e.

$$\bar{\phi}(n) = \langle \phi(t, \tau) \rangle = \frac{1}{T} \int_n^{n+T} \phi(t, \tau) d\tau \quad \forall n = 1, 2, \dots \quad (42)$$

where T is the cycle period in the fast time-scale τ , and n corresponds to the cycle number. Discrete values of $\bar{\phi}(n)$ are joined to obtain a continuous representation of the averaged response functions $\bar{\phi}(t)$. The cycle-averaged equations are defined for the evolution of any averaged variable $\partial(\bar{\phi})/\partial t$ subjected to a cycle-averaged applied load. For example, the evolution equation for the averaged shear strain rate is expressed as

$$\frac{\partial \bar{\gamma}^\alpha}{\partial t} = \dot{\gamma}_0^{*\alpha} \left| \frac{\bar{\tau}^\alpha - \bar{\tau}_{\text{kin}}}{\bar{g}^\alpha} \right|^{1/m} \text{sign}(\bar{\tau}^\alpha - \bar{\tau}_{\text{kin}}) \quad (43)$$

where $\gamma_0^{*\alpha}$ is a yet to be determined coefficient that is expected to be a function of time or other evolving variables. This coefficient is developed from considerations of the link between the averaged and the oscillatory solutions. The averaged rate $\partial(\bar{\phi})/\partial t$ is not dependent on the assumption of periodicity. As a one-dimensional illustration, consider a non-periodic function

$$\frac{\partial \phi}{\partial t} = t \sin(\omega t) \quad \text{with initial conditions } \phi(0) = 0 \tag{44}$$

The solution to this problem is

$$\phi(t) = \frac{-t \cos(\omega t)}{\omega} + \frac{\sin(\omega t)}{\omega^2} \tag{45}$$

The cyclic average of the solution is $\bar{\phi}(t) = 0$ and therefore $\partial\bar{\phi}/\partial t = 0$.

However, the application of the averaging operator $\langle \rangle$ on both sides of (44) yields

$$\left\langle \frac{\partial \phi}{\partial t} \right\rangle = -\frac{1}{\omega} \Rightarrow \bar{\phi}(t) = -\frac{t}{\omega} \neq 0$$

The procedure for defining the average equation (43) involves a calibration process that is explained below. To start with, consider the original uncoupled evolution equation for plastic shearing rate (4). This equation is solved using a single time integration process. Once the solution $\gamma^\alpha(t, \tau)$ is known, its cycle average $\bar{\gamma}^\alpha(t)$ is calculated, from which its rate of evolution, $[\partial\bar{\gamma}^\alpha(t)]/\partial t$, can also be calculated. Now, the parameter $\gamma_0^{*\alpha}$ can be calculated explicitly as

$$\gamma_0^{*\alpha} = \frac{\partial\bar{\gamma}^\alpha/\partial t}{\dot{\gamma}_0 |(\bar{\tau}^\alpha - \bar{\tau}_{kin})/\bar{g}^\alpha|^{1/m} \text{sign}(\bar{\tau}^\alpha - \bar{\tau}_{kin})} \tag{46}$$

Since the back stress τ_{kin}^α and the resolved shear stress τ^α always occur together as effective shear stress $\tau_{eff}^\alpha = \tau^\alpha - \tau_{kin}^\alpha$, the resolved shear stress and the back stress can be condensed into one single quantity. In general, $\gamma_0^{*\alpha}$ will depend upon both the average and the oscillations in τ_{eff}^α and g^α , i.e.

$$\gamma_0^{*\alpha} = f(\bar{\tau}^\alpha, \bar{\tau}^\alpha, \bar{g}^\alpha, \bar{g}^\alpha) \tag{47}$$

The functional dependence of $\gamma_0^{*\alpha}$ in equation (47) can be further reduced if the oscillations in the hardness variable are insignificant in comparison with the average hardness, i.e. $\bar{g}^\alpha \ll g^\alpha$. This assumption is supported by the solution of zero-order oscillatory problem (40), which shows that the oscillations in hardness are of order ϵ . This reduces the functional dependence equation (47) to

$$\gamma_0^{*\alpha} = f(\bar{\tau}^\alpha, \bar{\tau}^\alpha, \bar{g}^\alpha) \tag{48}$$

Furthermore, for most cyclic loading the change in \bar{g}^α within each cycle can be considered to be negligibly small. The case considered in this paper is focused on such cases. More general cases, where the change in hardness within each cycle is significant, will be presented in a future paper. Because of the form of equation (4), for problems where \bar{g}^α is almost constant within each cycle, $\gamma_0^{*\alpha}$ may also be assumed to be independent of \bar{g}^α . For such a case, $\gamma_0^{*\alpha}$ will vary for different slip systems if the material property $\dot{\gamma}_0$ for the slip systems varies. It should be noted that, if the change in average hardness \bar{g}^α within each cycle cannot be ignored, it will not be possible further to reduce the number of independent variables from equation (48). A special case of fully reversed loading (or the ratio $\tau^{zmin}/\tau^{zmax} \approx -1$), where this assumption of \bar{g}^α is not valid, is discussed in section 5 of this paper. However, for cases where the ratio τ^{zmin}/τ^{zmax} is not close to -1 , it is further possible to condense equation (48), which will be discussed below.

Next, to quantify the dependence of $\gamma_0^{*\alpha}$ on the resolved shear stress $\bar{\tau}^\alpha$, its oscillations are represented by characteristic parameters. For example, for a pure sinusoidal oscillation, a single parameter, namely the amplitude, is sufficient to represent the oscillatory behaviour. However, multiple parameters may be necessary for more complex waveforms. Thus, the functional dependence in equation (47) is quantified as

$$\gamma_0^{*\alpha} = f(\bar{\tau}^\alpha, \bar{\tau}^\alpha) = f(\bar{\tau}^\alpha, \bar{\tau}_{char1}^\alpha, \bar{\tau}_{char2}^\alpha, \bar{\tau}_{char3}^\alpha, \dots) \tag{49}$$

While in the present study only one parameter is used to characterize the oscillator, use of more parameters is being considered in future studies to improve accuracy. The function f is determined by crystal plasticity FEM simulations for a single crystal by a single-time-scale integration process for different values of $\bar{\tau}^\alpha$ and $\bar{\tau}^\alpha$. The average shear strain $\bar{\gamma}^\alpha$ and hence the average shear strain rate $\partial\bar{\gamma}^\alpha/\partial t$ are calculated from these simulations. Finally, $\gamma_0^{*\alpha}$ is calculated from equation (46) and is tabulated as a function of $\bar{\tau}$ and the oscillation amplitude $\bar{\tau}^{amp}$. From the table it is observed that $\gamma_0^{*\alpha}$ is actually dependent on the ratio $\bar{\tau}^\alpha/\bar{\tau}_{amp}^\alpha$. Since such a ratio will vary from 0 (zero average) to infinity (zero oscillation), the ratio is scaled to $\bar{\tau}^\alpha/(\bar{\tau}^\alpha + \bar{\tau}_{amp}^\alpha)$ or $0 \leq \bar{\tau}^\alpha/\bar{\tau}_{max}^\alpha \leq 1$. Figure 2 shows the variation in $\gamma_0^{*\alpha}$ with $\bar{\tau}^\alpha/\bar{\tau}_{max}^\alpha$. With knowledge of the average and the amplitude of the oscillation of τ^α , the parameter $\gamma_0^{*\alpha}$ can be obtained from this plot. This operation can decouple the two parts, enabling the solution of the averaged problem independently of the oscillatory problem.

From equation (49) it is clear that, to solve the average problem, the oscillatory resolved shear

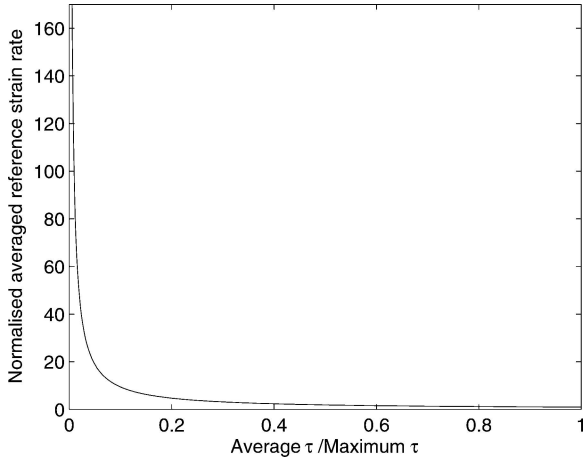


Fig. 2 Averaged reference slip rate (decoupling parameter) as a function of the averaged and oscillator parts of the resolved shear stress

stress has to be known. However, the oscillatory part is unknown *a priori* during the solution stage of the average problem. The oscillatory problem can be solved in a staggered manner with the average problem. However, the oscillatory problem needs small time increments. This coupling makes the method computationally prohibitive for simulations with a large number of cycles, and the computational gain over the single time integration is almost non-existent. Thus, instead of solving the oscillatory problem at each time increment of the average problem, the oscillations in the resolved shear stress τ^z are estimated. The asymptotic expansion helps in this process. Figure 3 shows the variation in average and the maximum τ^z in an active slip system in a typical grain of polycrystalline material. The change in the resolved shear stress τ^z is associated with

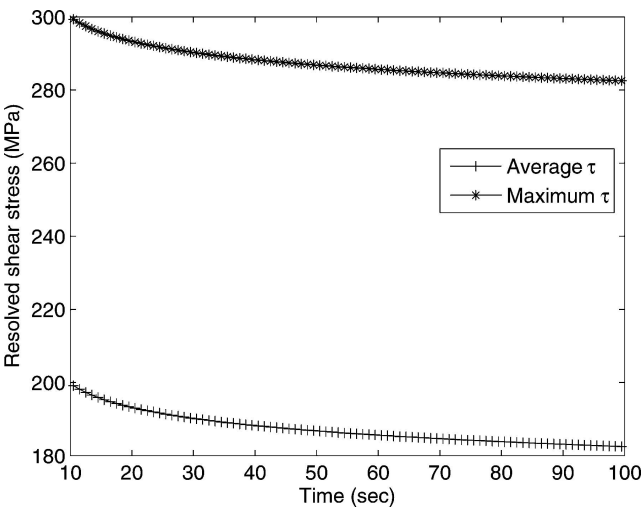


Fig. 3 Variation in average and maximum resolved shear stress in an active slip plane with time

plasticity. The variation in the averaged and maxima of resolved shear stress with time seems to follow a trend (see Fig. 3). It can be observed that the amplitude of the oscillation is more or less constant. This trend is explained by the asymptotics. Asymptotic expansions of equations (38) show that the zero-order oscillations in plastic variables are zero. As long as $\varepsilon \tilde{F}_{ij}^{p(1)} \rightarrow 0$, the response in the resolved shear stress oscillator $\tilde{\tau}^z$ is close to the elastic response, i.e. the oscillator with constant amplitude. The oscillations in the plastic variables will depend upon the ratio $\tau^{\min} / \tau^{\max}$. For $\varepsilon \tilde{F}_{ij}^{p(1)}$ to be large, large oscillations in shear strain rate are needed, for which $\tau^{\min} / \tau^{\max} \rightarrow -1$. If $\tau^{\min} / \tau^{\max} \neq -1$, then the oscillations in the plastic variables are extremely small, i.e.

$$\begin{aligned} \frac{\tau^{\min}}{\tau^{\max}} \rightarrow -1 &\Rightarrow \varepsilon \tilde{F}_{ij}^{p(1)} \rightarrow 0 \Rightarrow \varepsilon \tilde{\tau}^{\alpha(1)} \rightarrow 0 \Rightarrow \tilde{\tau}^{\alpha} \approx \tilde{\tau}^{\alpha(0)} \Rightarrow \tilde{\tau}^{\alpha} \\ &= \text{constant} \end{aligned} \tag{50}$$

Thus, with knowledge of the starting amplitude of the oscillation of resolved shear stress and the average resolved shear strain, the decoupling parameter $\gamma_0^{z\alpha}$ can be interpolated from the plot in Fig. 2.

The averaged evolution equations for hardness evolution are defined in a similar manner

$$\frac{\partial \bar{g}^{\alpha}}{\partial t} = \sum_{\beta}^{n_{\text{slip}}} \bar{h}^{\alpha\beta} \left| \frac{\partial \bar{\gamma}^{\beta}}{\partial t} \right| \tag{51}$$

where

$$\bar{h}^{\alpha\beta} = q^{\alpha\beta} \bar{h}^{\beta} \quad (\text{no sum on } \beta)$$

and

$$\bar{h}^{\beta} = \bar{h}_0^{\beta*} \left| 1 - \frac{\bar{g}^{\beta}}{\bar{g}_s^{\beta}} \right|^r \text{sign} \left(1 - \frac{\bar{g}^{\beta}}{\bar{g}_s^{\beta}} \right), \quad \bar{g}_s^{\beta} = \bar{g}_{s0}^{\beta} \left(\frac{\partial \bar{\gamma}^{\beta} / \partial t}{\dot{\gamma}_0} \right)^c \tag{52}$$

Again, the decoupling parameter $\bar{h}_0^{\beta*}$ is calculated from the solution of single time integration of a single crystal model for a wide range of loads. The decoupling parameter $\bar{h}_0^{\beta*}$ is found to depend on

$$\bar{h}_0^{\beta*} = f(\bar{g}^{\alpha}, \bar{\tau}^{\alpha}, \bar{\tau}^{\alpha}) \tag{53}$$

For an oscillator that can be characterized by the amplitude alone, the dependence can be expressed as

$$\bar{h}_0^{\beta*} = f \left(\bar{g}^{\alpha}, \frac{\bar{\tau}^{\alpha}}{\bar{\tau}^{\alpha\max}} \right) \tag{54}$$

Figure 4 shows a two-dimensional grid of average hardness \bar{g}^z and $\bar{\tau}^z / \bar{\tau}^{z\max}$, which is used to interpolate the decoupling parameter $\bar{h}_0^{\beta*}$.

The back stress evolution equation in (37) has the coupling between the average and the oscillator

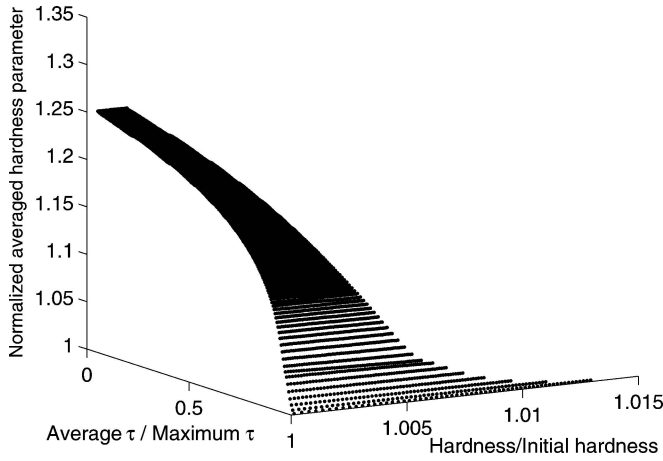


Fig. 4 Averaged reference hardness evolution (decoupling parameter) as functions of (a) averaged and oscillator parts of the resolved shear stress and (b) averaged and oscillator parts of the hardness

through only the rate of shear strain $\dot{\gamma}^\alpha$ and $|\dot{\gamma}^\alpha|$. Since half of this decoupling is already accomplished in equation (43), it was found that no additional steps are needed and its averaged evolution equation takes the form

$$\frac{\partial \bar{\Omega}^\alpha}{\partial t} = c \frac{\partial \bar{\gamma}^\alpha}{\partial t} - d \bar{\Omega}^\alpha \left| \frac{\partial \bar{\gamma}^\alpha}{\partial t} \right| \quad (55)$$

In conclusion, once the averaged solution for all the evolving variables are obtained in the CPFEM model, the dual-time-scale total solution is obtained by superposing different orders of the oscillatory solution for convergence to the true solution. It should also be noted that, during the reduction of the functional dependences from equation (48) to equation (49), and to estimate the oscillatory resolved shear stress from equation (50), it was assumed that the ratio $\tau^{\alpha \min} / \tau^{\alpha \max}$ is not close to -1 . The special load case where $\tau^{\alpha \min} / \tau^{\alpha \max} \rightarrow -1$ will be discussed in the next section.

5 CONSIDERATIONS FOR FULLY REVERSED LOADING ($R = -1$)

When the applied oscillatory load has a zero mean, the ratio of minimum to maximum resolved shear stresses ($\tau^{\alpha \min} / \tau^{\alpha \max}$) in any slip system will tend to towards -1 . Under such loading conditions, the average IBVP will have boundary conditions of zero traction on the surface on which the load is applied. In this case, the initial conditions of the average IBVP equation (36) serve as the sole driving force for the problem. The effective constitutive laws developed

in the previous section will still lead to the average solution. However, some modifications are necessary in the representation of the decoupling parameter $\dot{\gamma}_0^*$ in equation (46). It should be noted that $\dot{\gamma}_0^*$ approaches a singularity as $\bar{\tau}^\alpha - \bar{\tau}_{\text{kin}}^\alpha \rightarrow 0$. Thus, the decoupling parameter is redefined as $\dot{\gamma}_0^* |\bar{\tau}^\alpha - \bar{\tau}_{\text{kin}}^\alpha|$ and is explicitly expressed as

$$\dot{\gamma}_0^* |\bar{\tau}^\alpha - \bar{\tau}_{\text{kin}}^\alpha| = \frac{|\partial \bar{\gamma}^\alpha / \partial t|^m \text{sign}(\partial \bar{\gamma}^\alpha / \partial t)}{\dot{\gamma}_0 |1/\bar{g}^\alpha|} \quad (56)$$

The functional dependence of the decoupling parameter in equation (48) cannot be further reduced in this case. It will depend on the average value and oscillations of the resolved shear stress and the average hardness as shown in equation (48). Similarly, the decoupling parameter for the hardness evolution \bar{h}_0^* is redefined as $\bar{h}_0^* |\partial \bar{\gamma}^\beta / \partial t|$ for avoiding the singularity as $|\partial \bar{\gamma}^\beta / \partial t| \rightarrow 0$. Again, the functional form in equation (53) cannot be reduced to equation (54). Given the average resolved shear stress $\bar{\tau}^\alpha$, the average slip system hardness \bar{g}^α , and the oscillatory resolved shear stress $\tilde{\tau}^\alpha$, the decoupling parameters can again be calculated from a calibration process.

As discussed before, the value of $\tilde{\tau}^\alpha$ is not known during the solution of the average IBVP. The first-order oscillatory resolved shear stress cannot be ignored owing to large oscillations of plastic variables, and hence its amplitude cannot be taken as constant. Thus, for $\tau^{\alpha \min} / \tau^{\alpha \max} \rightarrow -1$, $\varepsilon \tilde{F}_{ij}^{p(1)} \rightarrow 0$ and $\varepsilon \tilde{\tau}^{\alpha(1)} \rightarrow 0$. Consequently, $\tilde{\tau}^\alpha \approx \bar{\tau}^{\alpha(0)} + \varepsilon \tilde{\tau}^{\alpha(1)}$ evolves with increasing cycles in the loading history. From equations (48) and (53) it can be inferred that the value of $\tilde{\tau}^\alpha$ in each cycle is required in order to decouple the average and oscillatory problems. An additional equation, corresponding to the evolution of the oscillatory resolved shear stress, is introduced to evaluate the value of $\tilde{\tau}^\alpha$. By taking the time derivative on both sides of equation (43) and rearranging variables, the following functional dependence on the rate of evolution of the oscillatory resolved shear stress can be established

$$\frac{\partial \tilde{\tau}_{\text{char}}^\alpha}{\partial t} = f \left(\tilde{\tau}_{\text{char}}^\alpha, \bar{g}, \frac{\partial \bar{g}^\alpha}{\partial t}, \bar{\tau}^\alpha, \frac{\partial \bar{\tau}^\alpha}{\partial t}, \frac{\partial^2 \bar{\gamma}^\alpha}{\partial t^2} \right) \quad (57)$$

Solution of the differential equation (57) provides the current value of $\tilde{\tau}^\alpha$ required by the average constitutive equations (46), (51), and (55). However, as the ratio $\tau^{\alpha \min} / \tau^{\alpha \max} \rightarrow -1$, the average values of different variables are considerably smaller compared with the oscillators. For example, the average resolved shear stress and its rate, $\bar{\tau}^\alpha$ and $\partial \bar{\tau}^\alpha / \partial t$, and the average slip rate, $(\partial^2 \bar{\gamma}^\alpha) / \partial t^2$, are very small. A numerical sensitivity analysis also corroborates this observation, and

the dependence of $\partial \bar{\tau}_{\text{char}}^\alpha / \partial t$ on $(\bar{\tau}^\alpha, \partial \bar{\tau}^\alpha / \partial t, (\partial^2 \bar{\tau}^\alpha) / \partial t^2)$ is consequently ignored. Thus, equation (57) is reduced to

$$\frac{\partial \bar{\tau}_{\text{char}}^\alpha}{\partial t} = f\left(\bar{\tau}_{\text{char}}^\alpha, \bar{g}, \frac{\partial \bar{g}}{\partial t}\right) \quad (58)$$

The variation of rate of change of oscillatory resolved stress with the oscillatory resolved stress and the average hardness is shown in Fig. 5. The average constitutive equations (46), (51), and (55), together with the evolution of the equation for the oscillatory shear stress (equation (58)), are solved during the solution of the average IBVP by a backward Euler algorithm for the case $R \rightarrow -1$. It should be noted that, for applied loads with a non-zero mean, equation (58) will be trivial because of the constant oscillator in equation (50).

6 NUMERICAL EXAMPLE

This dual-time-scale algorithm is used to study the deformation response of polycrystalline titanium alloy Ti-6Al subjected to cyclic loading. The cyclic response is simulated using both the single-time-scale and the multiple-time-scale algorithm. The constitutive laws are implemented in the commercial finite element code MSC MARC [29] using the user-defined material routine interface HYPELA2. An implicit time integration scheme proposed in references [13] and [15] is used to integrate the constitutive equations. A unit cube of polycrystalline aggregate is modelled by discretizing the cube by 2744 elements. Eight-noded brick elements with selective reduced integration are used for this purpose. Each element in the FE model represents one grain of the polycrystalline aggregate and is assigned a specific orientation. The deformation has been observed to be very sensitive to the overall texture in earlier work [15–17]. Thus,

crystallographic orientations that are statistically equivalent to orientations obtained from orientation imaging microscopy (OIM) are used. Statistical equivalence in orientation, misorientation, and microtexture between the simulated and experimental microstructures is achieved by using a method developed and described in references [16] and [17]. Figure 6 shows the comparison between the experimentally observed microstructure and the statistically equivalent microstructure used in the simulations. The number of elements and thus the grains used in the FE model are chosen to yield convergence with respect to the macroscopic response, i.e. increasing the number of elements in the model does not change the macroscopic response. A stress-controlled loading case is studied in this paper. A pressure boundary condition is applied to the top face using the FORCER routine of MARC. The pressure profile applied is sinusoidal with a frequency of 1 Hz, a mean of 500 MPa, and the amplitude of 350 MPa, and the deformation response for 100 cycles is simulated.

For the single-time-scale simulation, the constitutive model outlined in section 2 is used. Because

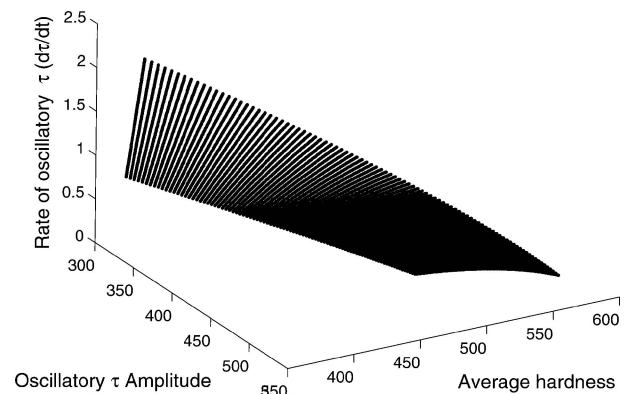


Fig. 5 Time rate of change of oscillatory resolved shear stress $\partial \bar{\tau}^\alpha / \partial t$ as a function of oscillatory shear stress $\bar{\tau}^\alpha$ and average slip system hardness \bar{g}^α

Table 1 Orthotropic elastic stiffness parameters for Ti-6Al

Elastic stiffness components	C_{11}	C_{12}	C_{13}	C_{33}	C_{55}
Value (GPa)	136.5	78.4	68.0	163.05	40.600

Table 2 Crystal plasticity parameters in the hcp model for Ti-6Al

CP parameters	Basal $\langle a \rangle$ slip	Prismatic $\langle a \rangle$ slip	Pyramidal $\langle c + a \rangle$ slip
γ_0	0.0023	0.0023	0.0023
m	0.02	0.02	0.02
g_0 (MPa)	322	320	846
h_0 (MPa)	100	100	350
r	0.5	0.5	0.55
n	0.14	0.1	0.1
g_s (MPa)	450	550	1650

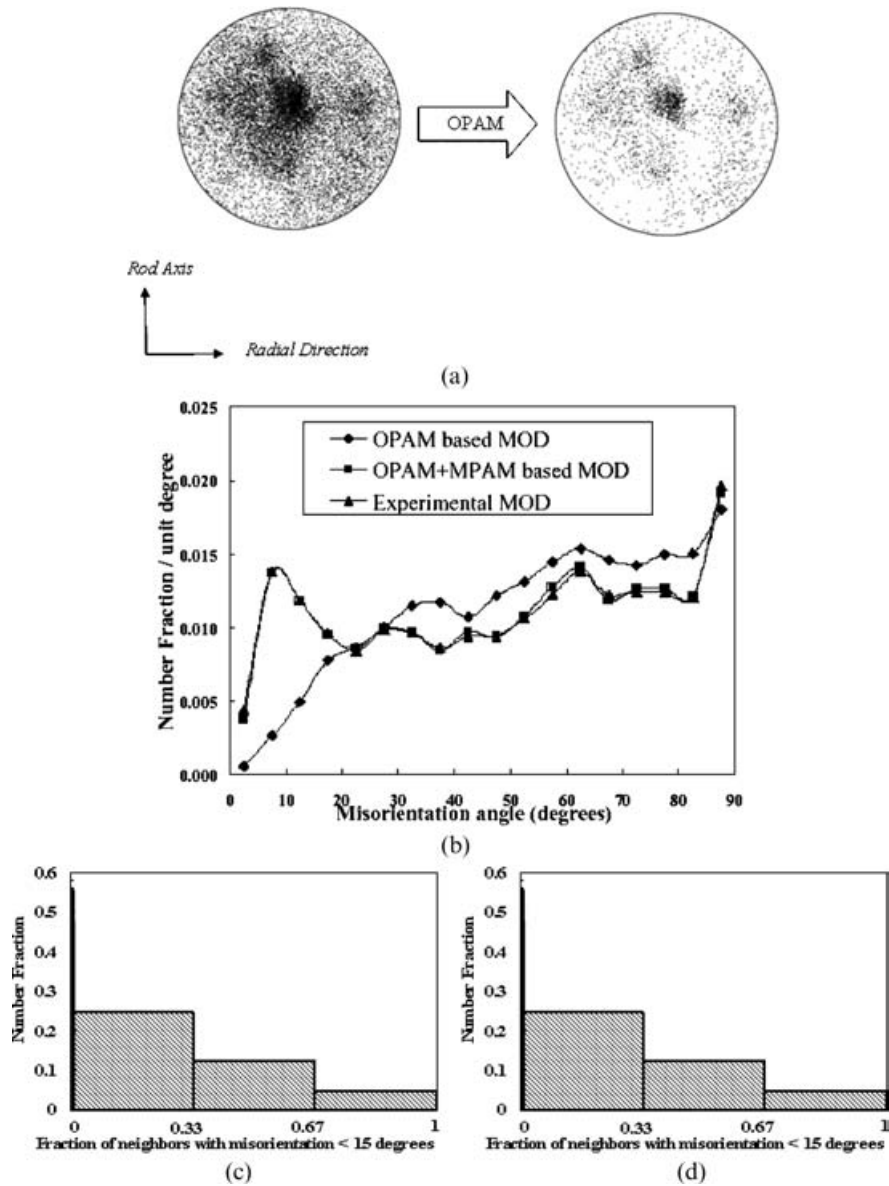


Fig. 6 Comparison of microstructures obtained experimentally (OIM) and by the statistically equivalent microstructure generation (OPAM + MPAM + MTPAM) method discussed in references [16] and [17]: (a) experimentally observed (0001) pole figure with 14 799 points and OPAM simulated inverse pole figure with 2744 points; (b) misorientation distribution; (c) experimental microtexture from OIM; (d) simulated microtexture

the applied loading is of high frequency, the single time integration simulation requires around 50 time increments for the solution for each cycle. The simulation took around 30 h on dual xeon processors of a cluster to analyse 100 cycles of pressure loading. In the multiscale algorithm, the average problem is solved using the effective constitutive equations outlined in section 4. In this problem, an average pressure of 500 MPa is applied. Since the loading is not oscillatory, the time increments required for the solution of the average problem is limited only by the accuracy of the implicit time integration [13] for

the effective constitutive equation. Thus, a typical time increment used for the averaged solution is as large as 2–3 times the time period of the sinusoidal pressure load. The average simulation took around 30 min to solve for 100 cycles. This is approximately a 60-fold computational gain when compared with single time integration. Figure 7 shows a comparison between the Cauchy stress contour by single time integration and the average solution at the beginning of the last (100th) cycle. It is evident from the contour plots that the solutions are in close agreement not only at macroscopic scale but at the grain level too.

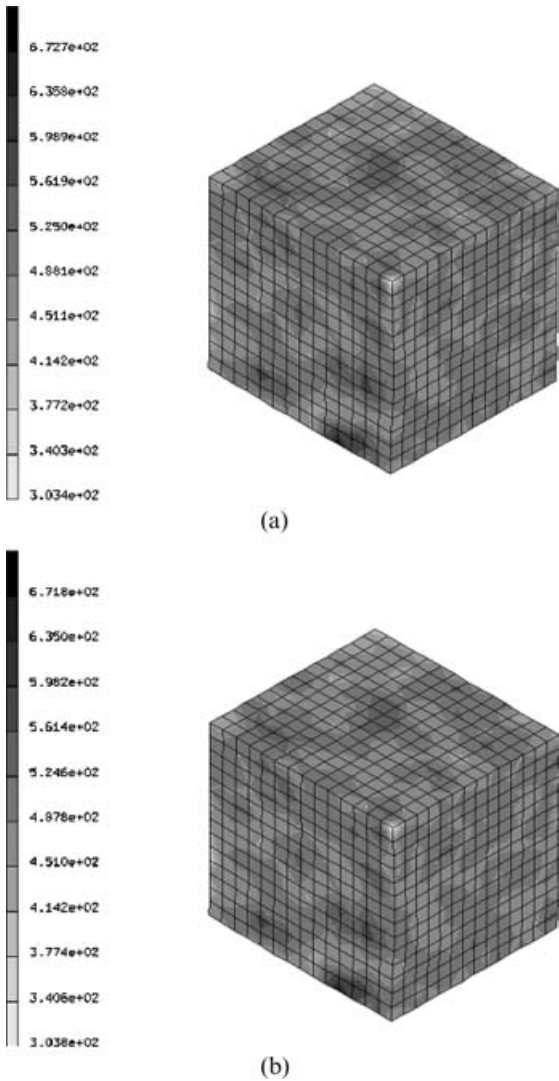


Fig. 7 Cauchy's stress contour at the beginning of the 100th cycle: (a) single-time-scale solution; (b) average solution

Upon obtaining the solution of the average problem, the oscillatory problems are solved for the last five cycles and superposed on the average solution to recover the total solution. Figure 8 shows the volume-averaged total strain in the loading direction in the polycrystalline aggregate obtained from the single-time-scale and multiple-time-scale solutions. The volume-averaged plastic strain in the loading direction with these two approaches is compared in Fig. 9. Excellent agreement is found in the time-averaged solutions. For comparison at the microscopic level, the shear slip in an active slip system at an integration point in an element by the two methods is plotted in Fig. 10. The dual-time-scale algorithm solution agrees very well with the single-time-scale solution at both macroscopic scale and grain level. The proposed two-time-scale

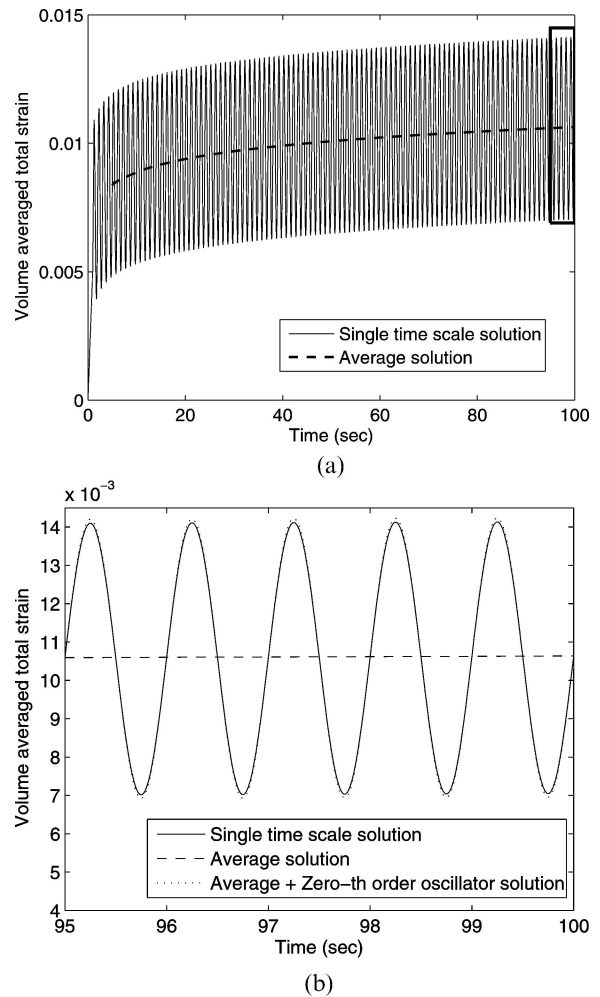


Fig. 8 Volume-averaged total strain in the loading direction

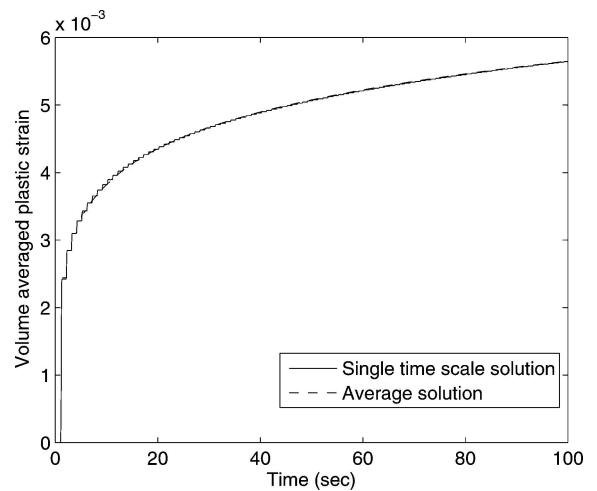


Fig. 9 Volume-averaged plastic strain in the loading direction

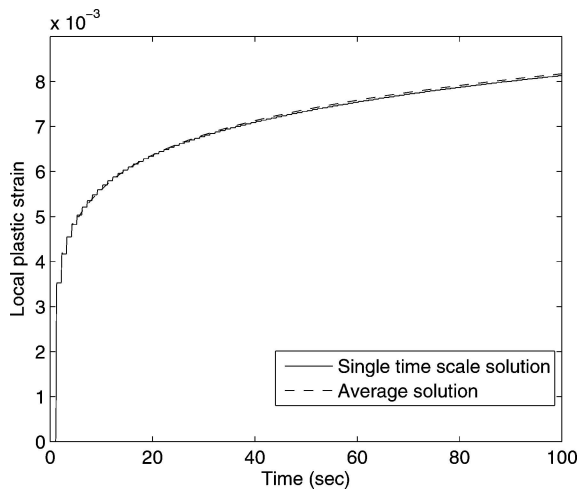


Fig. 10 Slip along an active slip plane at an integration point of an element

algorithm can achieve very high computational gain with almost no loss of accuracy for problems with cyclic loading and deformation.

As a final example, a case of cyclic deformation with fully reversed loading is studied. A sinusoidal pressure load of zero mean and an amplitude of 850 MPa is applied. Again, the solution of the average problem is able to follow the average solution of the total problem. Figure 11 shows the comparison of the volume-averaged plastic strain obtained by single time integration and the average problem. Since the loading is fully reversed, the average plastic strain will not vary much with the time, but the same is not true for the slip system hardness, which increases both while in positive loading and negative loading. This causes the slip system hardness to vary significantly with time, and the average problem is able to capture that, as shown in Fig. 12. Again, the

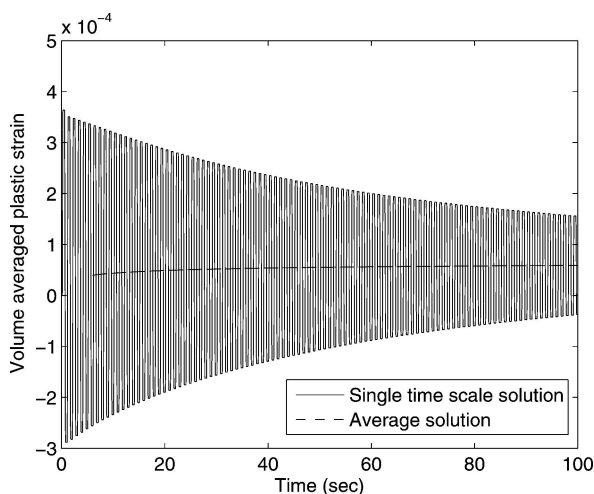


Fig. 11 Volume-averaged plastic strain in the loading direction for the fully reversed loading

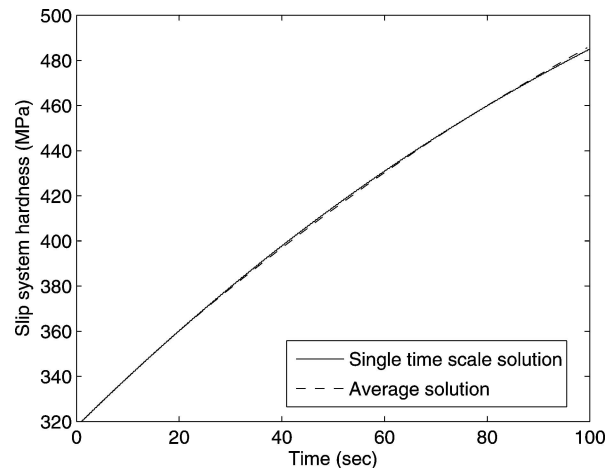


Fig. 12 Slip system hardness at an integration point of an element for the fully reversed loading

single-time-scale solution takes around 28 h to complete, while the average problem takes around an hour to execute.

7 CONCLUSIONS

A novel two-scale algorithm in the temporal domain is developed in this paper to study anisotropic plastic material response under cyclic loading. The algorithm is implemented for crystal plasticity constitutive equations. The initial boundary-value problem is decomposed into an uncoupled set of average problem and oscillatory problems. Effective constitutive equations are developed for the average problem in order to decouple the average and the oscillations. The resulting averaged constitutive equations do not rely on any assumptions of periodicity. The decoupling parameters in the averaged constitutive equations are calibrated from solving single grain problems with a single time-scale. Because the average problem is devoid of any oscillations, it can be solved with time increments that are of the order of multiple time periods of the cyclic loading. This leads to huge computational gain over the single-time-scale solution where the time increments are much smaller than the time period. The asymptotic expansion of various field variables is used further to decompose the oscillatory problem into various orders of oscillations. Each order of the oscillatory solution can be solved locally in the temporal domain with the knowledge of the averaged solution. The algorithm is validated by analysing the deformation response of polycrystalline Ti-6Al under high-frequency sinusoidal pressure. The results from multitime-scale solutions match very well with the

results obtained from single time integration, both at macroscopic scale and at grain level. On the other hand, the computational efficiency is enhanced by a factor of almost 60.

This multiscale analysis in time makes it possible to study the fatigue response of materials in an explicit manner for considerations of evolution of critical microstructural variables. It opens up the possibility of solving these problems for the entire fatigue life, in contrast to the extrapolation and empirical studies that are used presently [20]. The model presented in this paper is currently undergoing refinement for future work on the nucleation of fatigue cracks in polycrystalline materials.

REFERENCES

- 1 **Suresh, S.** *Fatigue of materials*, 1996 (Cambridge University Press, Cambridge).
- 2 **Coffin, L. F.** *Fatigue. Ann. Rev. Mater. Sci.*, 1973, **2**, 313–348.
- 3 **Laird, C. M.** The fatigue limit of metals. *Mater. Sci. Engng*, 1976, **22**, 231–236.
- 4 **Fleck, N. A., Kang, K. J., and Ashby, M. F.** The cyclic properties of engineering materials. *Acta Metall. Mater.*, 1994, **42**, 365–381.
- 5 **Hashimoto, T. M. and Pereira, M. S.** Fatigue life studies in carbon dual-phase steels. *Int. J. Fatigue*, 1996, **18**(8), 529–533.
- 6 **Paris, P. C.** The fracture mechanics approach to fatigue. In *Fatigue – an interdisciplinary approach*, 1964 (Syracuse University Press, Syracuse).
- 7 **Mineur, M., Villechaise, P., and Mendez, J.** Influence of the crystalline texture on the fatigue behaviour of a 316L austenitic stainless steel. *Mater. Sci. Engng*, 2000, **A286**, 257–268.
- 8 **Bennett, V. P. and McDowell, D. L.** Polycrystal orientation distribution effects on microslip in high cycle fatigue. *Int. J. Fatigue*, 2003, **25**, 27–29.
- 9 **Chu, R. Q., Cai, Z., Li, S. X., and Wang, Z. G.** Fatigue crack initiation and propagation in α -iron polycrystals. *Mater. Sci. Engng*, 2001, **313**, 61–68.
- 10 **Harren, S. V. and Asaro, R. J.** Nonuniform deformations in polycrystals and aspects of the validity of the Taylor model. *J. Mech. Phys. Solids*, 1989, **37**(2), 191–232.
- 11 **Mathur, K. K., Dawson, P. R., and Kocks, U. F.** On modeling anisotropy in deformation processes involving textured polycrystals with distorted grain shape. *Mech. Mater.*, 1990, **10**, 183–202.
- 12 **Kalidindi, S. R., Bronkhorst, C. A., and Anand, L.** On the accuracy of the Taylor assumption in polycrystalline plasticity. In *Anisotropy and localization of plastic deformation* (Eds J. P. Boehler and A. S. Khan), 1991, pp. 139–142 (Elsevier Science, New York).
- 13 **Kalidindi, S. R., Bronkhorst, C. A., and Anand, L.** Crystallographic texture evolution in bulk deformation processing of fcc metals. *J. Mech. Phys. Solids*, 1992, **40**, 537–569.
- 14 **Beaudoin, A. J., Mecking, H., and Kocks, U. F.** Development of local shear bands and orientation gradients in fcc polycrystals. In *Simulation of materials processing; theory, methods and applications, NUMIFORM'95* (Eds S. F. Shen and P. Dawson), 1995, pp. 225–230 (A. A. Balkema, Rotterdam).
- 15 **Hasija, V., Ghosh, S., Mills, M. J., and Joseph, D. S.** Modeling deformation and creep in Ti–6Al alloys with experimental validation. *Acta Mater.*, 2003, **51**, 4533–4549.
- 16 **Deka, D., Joseph, D., Ghosh, S., and Mills, M. J.** Crystal plasticity modeling of deformation and creep in polycrystalline Ti–6242. *Metall. Trans. A*, 2006 (in press).
- 17 **Venkatramani, G., Deka, D., and Ghosh, S.** Crystal plasticity based FE model for understanding microstructural effects on creep and dwell fatigue in Ti–6242. *Trans. ASME, J. Engng Mater. and Technol.*, 2006, **17A**(5), 1371–1388.
- 18 **Xie, C. L., Groeber, M., Butler, R., and Ghosh, S.** Computational simulations of tensile and fatigue tests of HSLA steel based on experiments. In *Proceedings of SAE World Congress*, 2003.
- 19 **Xie, C., Ghosh, S., and Groeber, M.** Modeling cyclic deformation of HSLA steels using crystal plasticity. *Trans. ASME, J. Engng Mater. Technol.*, 2004, **126**, 339–352.
- 20 **Sinha, S. and Ghosh, S.** Modeling cyclic ratcheting based fatigue life of HSLA steels using crystal plasticity FEM simulations and experiments. *Int. J. Fatigue*, 2006, **28**, 1690–1704.
- 21 **Turkmen, H. S., Loge, R. E., Dawson, P. R., and Miller, M.** On the mechanical behaviour of AA 7075-T6 during cyclic loading. *Int. J. Fatigue*, 2003, **25**, 267–281.
- 22 **Dawson, P. R.** Computational crystal plasticity. *Int. J. Solids Structs*, 2000, **37**, 115–130.
- 23 **Yu, Q. and Fish, J.** Temporal homogenization of viscoelastic and viscoplastic solids subjected to locally periodic loading. *Comput. Mechanics*, 2002, **29**, 199–211.
- 24 **Oskay, C. and Fish, J.** Multiscale modeling of fatigue for ductile materials. *Int. J. Multiscale Comput. Engng*, 2004, **2**, 1–25.
- 25 **Balasubramanian, S. and Anand, L.** Elastoviscoplastic constitutive equations for polycrystalline fcc materials at low homogeneous temperatures. *J. Mech. Phys. Solids*, 2002, **50**, 101–126.
- 26 **Asaro, R. J. and Rice, J. R.** Strain localization in ductile single crystals. *J. Mech. Phys. Solids*, 1977, **25**, 309–338.
- 27 **Harder, J.** Crystallographic model for the study of local deformation processes in polycrystals. *Int. J. Plasticity*, 1999, **15**, 605–624.
- 28 **Morrissey, R. J., McDowell, D. L., and Nicholas, T.** Microplasticity in HCF of Ti–6Al–4V. *Int. J. Fatigue*, 2001, **23**, S55–S64.
- 29 *MSC-MARC reference manuals*, 2005 (MSC Software Corporation, Santa Ana, CA).